Structure-Transport Relationships of Poly(Aryl Piperidinium) Anion-Exchange Membranes: Effect of Anions and Hydration

Xiaoyan Luo,[1] Santiago Rojas-Carbonell[2], Yushan Yan[2], and Ahmet Kusoglu*,[1]

[1] Energy Technologies Area, Lawrence Berkeley National Laboratory

1 Cyclotron Road, Berkeley CA 94720, USA

[2] Department of Chemical and Biomolecular Engineering, University of Delaware

Newark, DE 19710 USA

* Email: AKusoglu@lbl.gov

Abstract

Hydroxide-exchange membrane (HEM) fuel cells are emerging energy conversion technologies. A significant effort has been expended to develop new HEMs with enhanced transport functionality, which has driven the need for understanding how transport of hydroxide and other anions in these membranes is related to hydration and nano-morphology. In this work, we report the results of a systematic study on poly(aryl piperidinium)-based on terphenyl (PAP-TP-85), a HEM that previously showed promising fuel cell performance and durability. Membrane water uptake and anion conductivity in liquid and vapor water, as well as the impact of counter-anion forms on these properties, are investigated and compared with a commercial anion exchange membrane (AEM), Fumasep FAA3, and proton-exchange membranes (PEMs), Nafion and sPEEK. Different water uptake in liquid *vs.* saturated vapor is observed for both AEMs (i.e., PAP and FAA3), indicating *Schroeder's paradox*, regardless of anion form. Morphology of AEMs examined via small-angle X-ray scattering (SAXS) shows weak phase-separation, regardless of hydration level and anion type, which is attributed to the reduced chemical dissimilarity between the backbone and ionic moieties. Despite both AEMs' amorphous nanostructure, PAP-AEM has a higher ion conductivity than FAA3. Water content plays a more significant role than does temperature in controlling the anion conductivity in water vapor. In liquid water, normalized conductivity shows a universal dependence on hydration, regardless of the anion form. Moreover, in water vapor, ion mobility showed stronger impact than ion concentration to conductivity was found to primarily controlled by hydration. Thus, ion transport in disordered AEMs is governed primarily by hydration, in contrast to phase-separated ionomers, where ion transport is governed by nanostructure-hydration interplay. This study demonstrates the importance of hydration level and ion mobility for anion transport in amorphous AEMs and provides an understanding of parameters governing their transport properties.

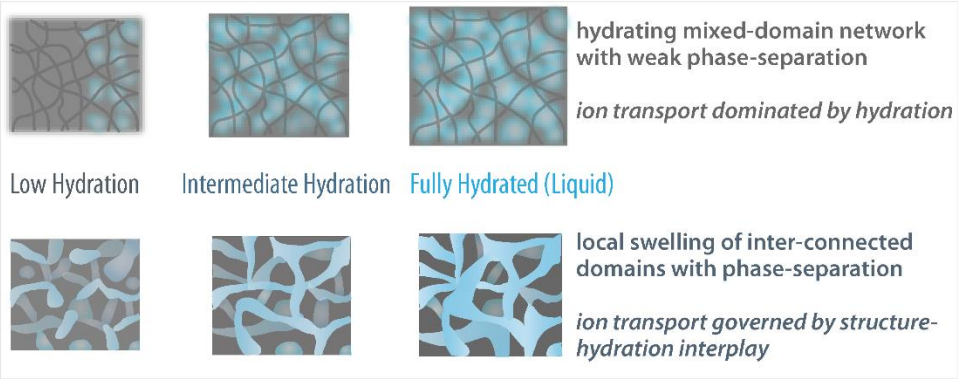

1. Introduction

Hydroxide exchange membrane (HEM) fuel cells (HEMFCs) offer the advantages of using less expensive electrocatalysts, bipolar plates and membranes than the conventional proton exchange membrane fuel cells (PEMFCs), hence they have attracted significant interest over the past 15 years.[1-2] Compared to the benchmark PEM-Nafion, where the functional group is a strong acid, HEMs generally show weaker electrolyte behavior due to their functional groups such as quaternary ammonium (QA), being weaker bases.[3-4] Research groups[5-13] in the HEM community have introduced various polymer chemical structures over the years aiming for high hydroxide conductivity and chemical stability under highly basic conditions and elevated temperatures. Recently, Wang *et al.* reported a HEM that yielded OH^- anion conductivity of 140 mS/cm at 80 °C with alkaline stability of 2,000 hrs in 1M KOH at 100°C, based on 3% decrease in IEC determined by potentiostatic titration.[14] Even though these efforts significantly improved HEM development, there is still a lack of standard commercial HEMs that provide long-term chemical stability over several thousand-hour run.[15-22]As the transport medium for both OH^- and water, the HEM is very critical in HEMFC water management. Poorly balanced water management largely hinders cell performance and durability.[23-26] HEMFC operation involves the generation of water on the anode and consumption of water at the cathode, in contrast to the PEMFCs. For each hydrogen molecule, the water generated on the anode of HEMFCs is twice as much as water generated in the cathode of PEMFCs whereas water is consumed due to the ORR on the cathode, which make water management extremely challenging.

A ubiquitous candidate for HEMFC is the separators based on anion-exchange membranes (AEMs), which contain positively charged functional groups allowing the transport of OH^- and other anions and water. AEM is among an emerging class of ion-conductive electrolyte which finds uses in many electrochemical systems, such as fuel cells,[27] electrolyzers,[28] redox flow batteries,[29] carbon-dioxide reduction systems,[30] and lithium-air batteries.[31] The water uptake kinetics of various AEMs was reported, and faster kinetics were observed with increasing temperature.[32] Benzimidazolium based AEM was found to have different interfacial water transport phenomena compared to a commercial membrane, Fumasep FAA3, a poly(arylene ether) AEM with QA functional groups.[33] Water sorption and water transport through an early generation commercial AEM, Tokuyama A201 membrane was found to have the same order of magnitude of water diffusivity as Nafion.[34] Water and ion diffusivity of A201 in HCO_3^- form were studied using PFG-NMR.[35] Despite studies on water uptake of AEMs using multiple experimental techniques, morphological investigations are needed to correlate hydration and transport properties. Techniques such as small- and wide-angle X-ray scattering (SAXS and WAXS) as well as atomic force microscopy (AFM) have been employed to study the morphology of AEMs.[36-41] Kreuer *et al.*[4] reported morphology of Fumasep FAA3 in Br^- and OH^- forms differ, which was attributed to the different degree of ion dissociation. Schibli *et al.*[37] studied the morphology of benzimidazole-based AEM in Cl^- and I^- form using SAXS/WAXS in various conditions. They identified three length scales in the polymer: ion-polymer spacing (4Å), polymer-polymer inter-chain spacing (6 Å), and an intra-chain repeat distance (20 Å), but with no long-range order at higher length scales. To design new membranes with improved levels of anion conduction, it is important to understand the parameters influencing membrane anion conductivity, including polymer chemistry, structure, and hydration level. The transport properties are associated with the anion/water interaction and the hydrophilic domains' size, fraction and connectivity, all of which are driven by hydration, and interrelated to the ionic moieties within the hydrophilic phase.[39, 42-43] While transport and sorption properties of AEMs are routinely measured in liquid water, their characterization in controlled humidity is rather nascent, which limits the current understanding of the role of hydration. The key is to delineate the interplay between the humidity-driven changes in water uptake and anion-induced changes in membrane hydration, and how they collectively influence the AEM's structure-transport relationship.

The goal of this article is to explore the complex interplay of anion conduction, membrane hydration, and its nanostructure. Water uptake behavior and anion transport of AEMs in Cl^-, Br^-, I^-, OH^-, CO_3^{2-}, HCO_3^-, and SO_4^{2-} were examined in liquid and vapor phase water, and compared with PEMs. Nano-morphology of the hydrated membranes in various anion forms were probed *in-situ* using SAXS. Poly (aryl piperidinium) based on terphenyl (PAP-TP-85), (as shown in Scheme 1), an AEM that has shown promising cell performance,[14] is chosen for systematic analysis and compared with a commercial non-cross-linked Fumasep FAA3. Nafion and sPEEK are also used for comparison, where possible.

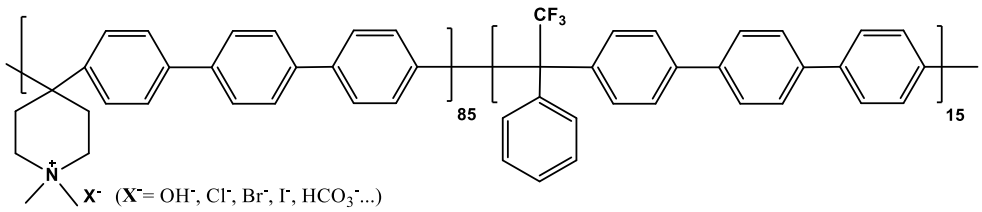

Scheme 1 Chemical structure of PAP (PAP-TP-85) membranes

2. Experimental

2.1 Materials

PAP-TP-85 membranes were prepared according to a recent publication[14] (and abbreviated as PAP). Non-reinforced Fumasep FAA3 membranes (Br^- form) were received from Fumatech and abbreviated as FAA3. Proton form Nafion and sPEEK membranes were purchased from Fuel Cell Store. NaCl, NaBr, NaI, NaOH, Na_2CO_3, $NaHCO_3$, and Na_2SO_4 salts were purchased from Sigma Aldrich and used as-received. Each counter-ion form (i.e., Cl^-, Br^-, I^-, OH^-, CO_3^{2-}, HCO_3^-, and SO_4^{2-} forms) of membrane was obtained separately by soaked twice in 1M 200 mL corresponding ion salt solution with molar ratio of M_{salt}: $M_{membrane}$> 1000:1 for at least 4 days and followed by washing with DI water (18.5 MΩ, Millipore water) to remove residual ions. Membranes in OH^- form and in other counter-ion forms were stored in an Ar purged cell and DI water, respectively, prior to use.

2.2 Membrane Conductivity

Membranes with different anion forms were cut into rectangles with dimensions of 10 mm × 35 mm. A four-probe in-plane conductivity cell was used for conductivity measurements. Linear sweep voltammetry (BioLogic VSP) was used to measure the membrane resistance in liquid water

at ambient conditions. For conductivity in water vapor, a membrane testing system (MTS 740, Scribner Associates Inc.) equipped with a Solartron 1286 DC potentiostat was used under controlled temperatures. Membrane ion conductivity κ was calculated from:

$$\kappa = \frac{L}{R \times A} \tag{1}$$

where L is the distance of two Pt electrodes for measuring voltage, R is the membrane resistance, and A is the cross-sectional area of the membrane.

2.3 Membrane Density

An Ohaus density determination kit was used to determine the dry density of the membranes (ρ_{dry}) at room temperature. All the membranes were dried in a vacuum oven overnight and then cooled to room temperature prior to measurement. An Ohaus Adventurer® balance was used to obtain the sample mass in air and in the auxiliary liquid (i.e., decane). The sample dry density was calculated according to:[44]

$$\rho_{\mathrm{dry}} = \frac{W_A}{W_A - W_B}(\rho_0 - \rho_L) + \rho_L \tag{2}$$

where W_A and W_B are the sample weight in air and in the auxiliary liquid. ρ_0 and ρ_L are the density of the auxiliary liquid and air, respectively.

2.4 Water-sorption Behavior

Isothermal water vapor sorption of the membrane was measured using a dynamic vapor sorption analyzer (DVS Surface Measurement Systems, UK) with temperature and humidity control. The samples were humidified from 0 to 98% RH, and then dehumidified from 98% to 0% with increments of 10% RH at 25 °C. The humidified membrane weight (W_{RH})was determined at each RH step after the mass gain reached a steady state. The dry weight (W_{dry}) of the humidified membrane was obtained after drying the anion-exchange membrane at 0% RH at 25 °C in the DVS. The details of the experimental procedure can be found in a previous study.[45] The percent water uptake (WU) by weight was calculated from the measured weight:

$$WU = \frac{W_{RH} - W_{\mathrm{dry}}}{W_{\mathrm{dry}}} \times 100 \tag{3}$$

From the water uptake measured during sorption, WU_{sorption}, and desorption, $WU_{\text{desorption}}$, sorption hysteresis in vapor phase (Δ_{WU}) was calculated as follows:

$$\Delta_{WU} = WU_{\text{desorption}} - WU_{\text{sorption}} \tag{4}$$

In addition, liquid water sorption measurement was carried out by soaking the membrane in liquid water for at least three days and then measuring its wet weight (W_{wet}), after blot dried the surface water. Dry weight (W_{dry}) of the wet membrane was determined after vacuum drying the samples at 110 °C overnight and cooling in a desiccator, and water uptake in liquid water is calculated using Equations (3). To characterize hydration, water content, λ, is calculated from the average of water uptake during sorption and desorption:

$$\text{Water Content } (\lambda) = \frac{\text{mol } H_2O}{\text{mol Ion}} = \frac{WU}{IEC \times M_{H_2O}} \tag{5}$$

where IEC (mmol/g) is the ion exchange capacity and M_{H_2O} is the molar mass of water (18 g/cm^3). Water volume fraction was calculated based on the following equation:

$$\phi_{\text{w}} = \frac{V_{H_2O}}{V_{H_2O}+V_p} = \frac{\frac{W_{wet}-W_{dry}}{\rho_{H_2O}}}{\frac{W_{wet}-W_{dry}}{\rho_{H_2O}}+\frac{W_{\text{dry}}}{\rho_{\text{dry}}}} = \frac{18\lambda}{18\lambda+\frac{1}{IEC\rho_{\text{dry}}}} \tag{6}$$

where W_{wet} and W_{dry} are the weight of wet and dry membrane, respectively, and ρ_{H_2O} and ρ_{dry} are the density of water and dry membrane, respectively. For the density of membranes, the measured values (from Eq. 2) are used.

Thermal gravimetric analysis (TGA 4000) and differential scanning calorimetry (DSC, PerkinElmer 8000) were used to estimate the values of free water (λ_f) and nonfreezable water (λ_{nf}).[46-48] Fully hydrated membranes were blot-dried with Kimwipe and loaded into TGA with initial wet mass of the sample (W_{wet}) and then heated in a N_2 atmosphere from 30 to 700 °C at 10 °C/min. The weight of dry membranes (W_{dry}) was determined from the point at which degradation of hydrophilic groups in the polymers. The total water content of membrane (λ_t) was calculated using Equation 3. The fraction of freezable water (W_f) was determined using DSC equipped with a cooling apparatus. Prior to test, DSC was calibrated against indium and decane and then a baseline run recorded with empty samples pans. Samples were blot-dried with Kimwipe

and quickly sealed in aluminum DSC pans with sample mass of ~ 7 mg measured on an analytical balance. The DSC curves were obtained under N_2 atmosphere from -50 to 50 °C at a scanning rate of 2 °C/min. The freezable water content was calculated using the following equation:

$$\lambda_f = W_f\,(\%) \times \lambda_t = \frac{\Delta H_{mem}}{\Delta H^0_{m,H_2O}} \times \lambda_t \quad (7)$$

where ΔH_{mem} and $\Delta H^0_{m,H_2O}$ are the enthalpy change of membranes and pure water (314 J/g), respectively. ΔH_{mem} was calculated by integrating the area under the cooling curve.

Nonfreezable water content, λ_{nf} was calculated as follows:

$$\lambda_{nf} = \lambda_t - \lambda_f \quad (8)$$

2.5 Membrane Swelling

The membrane through-plane swelling ratio was calculated from the thickness changes using a Heidenhain ND 200 length gauge as follows:

$$\text{Swelling ratio} = \frac{L_{\text{wet}} - L_{\text{dry}}}{L_{\text{dry}}} \times 100\% \quad (9)$$

where L_{wet} and L_{dry} are the thicknesses of the equilibrated membrane in wet and dry state, respectively. L_{wet} was obtained after soaking the membrane in liquid water for at least 3 days. L_{dry} was taken after drying the sample with N_2 gas to a constant dry thickness.

2.6 Small Angle X-ray Scattering (SAXS)

Small-angle X-ray scattering (SAXS) experiments were performed in beamline 7.3.3 of the Advanced Light Source (ALS) at Lawrence Berkeley National Laboratory (LBNL). The X-ray wavelength used was $\lambda = 0.124$ nm, with a monochromator energy resolution of E/dE of 100, and the presented patterns were collected using a 2D Dectris Pilatus 2M CCD detector (172 μm × 172 μm pixel size). The scattering wave vector, $q = 4\pi \sin(\theta/2)/\lambda$, where θ is the scattering angle, was in the range of 0.001 to 0.04 $Å^{-1}$ for SAXS. SAXS images for dry and liquid-equilibrated samples were obtained *in-situ* using custom-designed temperature-controlled solution cells with X-ray transparent Kapton™ windows. Dry samples were sealed in sample holders after vacuum drying

for 12 hr. For liquid-water experiments, samples were immersed in liquid water in the solution cells. All the experiments were carried out at 25 °C, and the samples were equilibrated at least 2 hr prior to imaging. The collected two-dimensional scattering patterns were azimuthally integrated to generate 1-D intensity profiles, I(q), which were corrected for background scattering. Hydrophilic-domain spacing and inter-crystalline spacing are calculated by using a Gaussian fit to the peaks obtained from SAXS.

3. Results and Discussion

3.1 Small-angle X-ray scattering

The phase-separation of polymeric and aqueous domains within a hydrated ionomer gives rise to a scattering peak in SAXS experiments. In the SAXS spectra of most hydrated PEMs, such as Nafion, this peak is usually assigned to a hydration-dependent "ionomer peak", corresponding to a characteristic hydrophilic water-domain spacing of 3 to 6 nm, as shown in Figure 1. A so-called matrix knee appears between q = 0.02 - 0.1 $Å^{-1}$, which corresponds to the inter-crystalline spacing between 10 and 25 nm. sPEEK is used for comparison due to its similar chemical structure to PAP. For the two hydrated AEMs studied herein (PAP and FAA3), and sPEEK, only a very broad, weak peak is observed in the q range of 0.03 to 0.07 $Å^{-1}$. The absence of peaks indicates that these AEMs lack a detectable degree of phase-separation, which could be explained by the reduced chemical dissimilarity between the aromatic stiff backbone and ionic moieties. This phenomenon could be also attributed to the fact that the functional groups are directly attached to the polymer backbone, instead of via a long side-chain as in Nafion, which reduces the polymer domains' tendency to phase separate. Similar results were reported by Schibli *et al.*,[37] who showed that SAXS of a benzimidazole-based AEM, in which the functional group is part of the polymer backbone, did not show any nanoscale phase separation. Even though both AEMs lack a strong phase-separation, a broad ionomer peak for PAP (Figure 1a) appears at a slightly higher q value compared to FAA3 samples, which could be attributed to their different degree of anion dissociation. In addition, unlike Nafion and other PFSAs, which show hydration-dependent d-spacing,[49] the nano-morphology of the AEMs does not change much upon hydration and counter-anion form (Figure S1, a to b and c to d). Similarly, heating in liquid water does not alter the nano-morphology of PAP, which indicates that the weak structural order arising from a lack of electrostatic interactions does not change with temperature (Figure 1b).

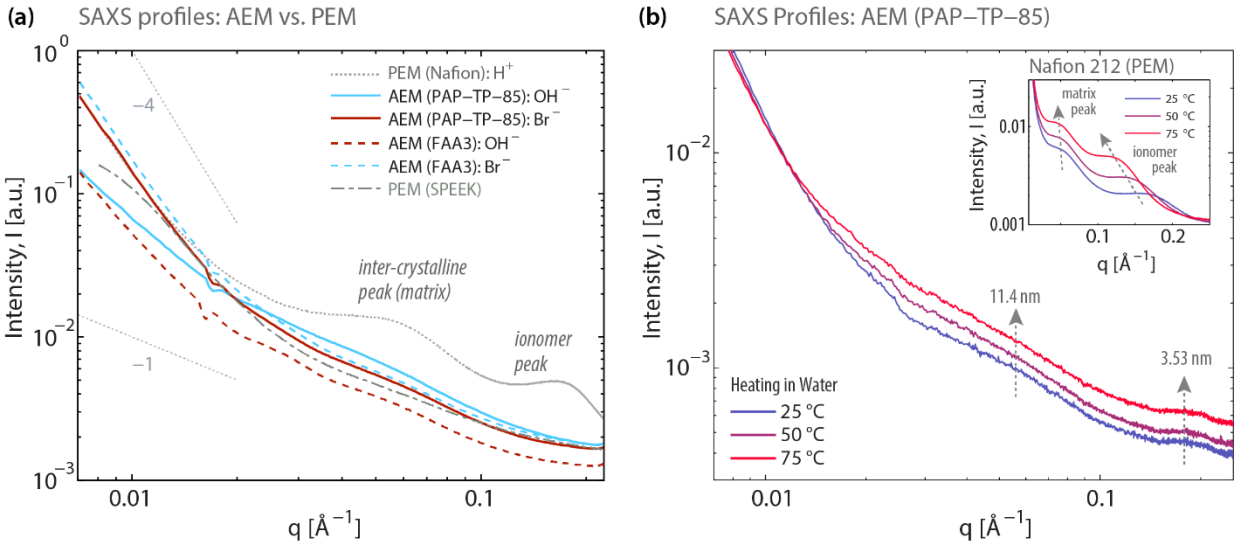

Figure 1 (a) Small-angle X-ray scattering comparison for two AEMs (PAP and FAA3), sPEEK and Nafion 211; (b) The impact of temperature on the SAXS profiles of PAP.

3.2 Water sorption

3.2.1 Liquid and water vapor sorption

In terms of AEM chemistry, PAP has a higher λ than FAA3 for each counter-anion form, due to the higher ion exchange capacity (IEC) of the former. This higher water content of PAP than FAA3 can also be seen from water vapor sorption (see Figure 3 b), In addition, in OH^- form, both AEMs exhibit higher λ compared to sPEEK (H^+) PEM (IEC= 1.45 mmol/g), which could be attributed to higher IEC of these AEMs (Table 1).

The different types of water in the membrane are quantified using the DSC and TGA shown in SI (Figure S5), from which freezable (λ_f) and nonfreezable water (λ_{nf}) are determined, as in Table 2. λ_f is significantly lower than λ_{nf} for both membranes, in good agreement with a previous report.[50] PAP has a λ_f of 2.1 (mol(H_2O)/mol(ion)), which is higher value FAA3's λ_f of 0.02, which is also in line with the trends shown in Figure 2a.

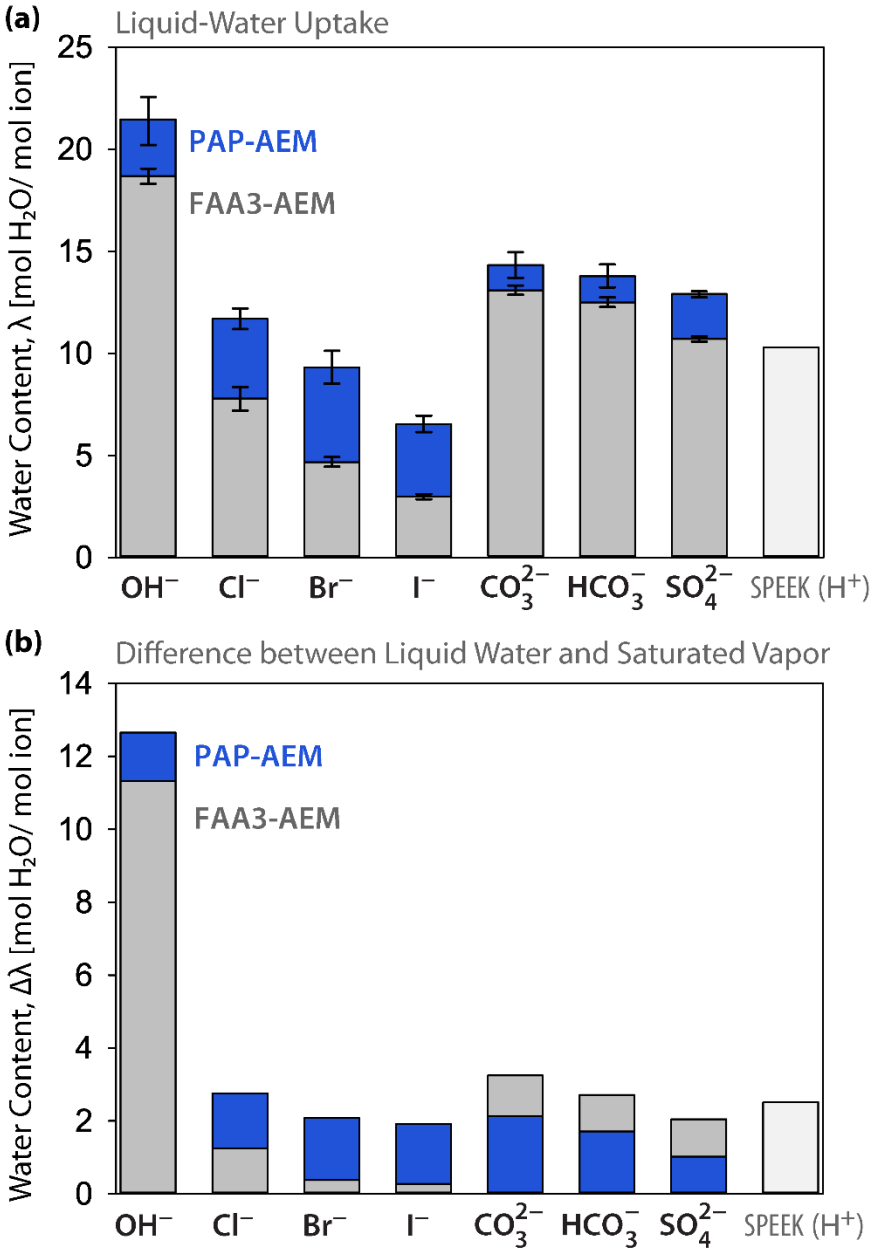

Figure 2 (a) Liquid-water content of PAP and FAA3 in different anion forms compared to sPEEK at room temperature and (b) water content difference (Δλ) for membranes in liquid water and saturated water vapor (Schroeder's paradox).

Table 1 Aqueous equivalent conductivities (κ_o) and diffusion coefficients (D_{x^-}) of ions in infinite dilution[51] and ion exchange capacity (IEC) and density of the AEMs in different anion forms

Counter-anion	Reference D_{x^-} * ($\times 10^5$ cm^2/s)[51]	Reference Ionic Conductivity, κ_o * (S cm^2/mol) [51]	PAP-IEC (mmol/g)	FAA3-IEC (mmol/g)	PAP-Dry Density (g/cm^3)	FAA3-Dry Density (g/cm^3)
-OH$^-$	5.27	198	2.35	1.91	1.22	1.31
-Cl$^-$	2.03	76.31	2.25	1.85	1.17	1.28
-Br$^-$	2.08	78.1	2.05	1.71	1.22	1.22
-I$^-$	2.05	76.8	1.87	1.58	1.43	1.46
-HCO$_3^-$	1.19	44.5	2.13	1.81	1.30	1.46
-CO$_3^{2-}$	0.92	69.3	2.13	1.81	1.17	1.28
-SO$_4^{2-}$	1.07	80	1.98	1.75	1.17	1.22

* Diffusion coefficients and ionic conductivity at infinite dilution of anions.[51]

Table 2 Freezable and nonfreezable water in the membranes

Membrane	λ_f (mol H$_2$O/mol ion)	λ_{nf} (mol H$_2$O/mol ion)
PAP(CO$_3^{2-}$)	2.1	15.5
FAA3(CO$_3^{2-}$)	0.02	16.8

Figure 3a summarize sorption behavior of AEMs in different anion forms in terms of water content, λ, as a function of relative humidity (RH). Additional data on water uptake behavior of FAA3 can be found in Figure S2 in Appendix. Overall, membranes exhibit a typical sigmoidal shaped water-sorption isotherm that was commonly observed in PFSA membranes and other reported AEMs.[32, 42, 52] At very low RH (<10%), membrane water content increases rapidly with RH, which could be attributed to the flexibility of the polymer matrix and its affinity to water.[52] At intermediate RH (10-70%), the sorption isotherm is quasi-linear, and the ionic groups in the polymers show the strongest interaction with water molecules.[53] Above 70% RH, the sorption isotherm displays highly nonlinear upturn with RH, due to the increasing amount of bulk ("free") water.

The strong effect of counter-anion on the water content of PAP and FAA3 at a given RH in the vapor is similar to that observed in liquid water in Figure 2a, as well as in line with the recent

simulation findings.[43] The membranes in HCO_3^- and CO_3^{2-} forms stand out from those in the other ion forms with their much higher λ, and this can be attributed to the fact that carbonate ions have stronger hydrogen bonds with water than water among themselves. This strong interaction reduces the mobility of the water in the hydration shell.[54] Between HCO_3^- and CO_3^{2-} forms (Figure 3b), both AEMs show almost identical water content, indicating a lesser effect of ion valance. This result is consistent with observations for water uptake of cation-exchanged Nafion, which was shown to exhibit less dependence on the cation valence than to the cation size.[42] The water content of halides decreases in the order of their ionic radius, $I^- < Br^- < Cl^-$, which agrees with a previous study,[4] wherein the difference was attributed to their order of dissociation enthalpies of the corresponding salts (*i.e.*, the more exergonic the dissolution of the ion pair, the more ions will dissociate at a given RH, resulting in increased osmotic pressure and corresponding to higher water content).

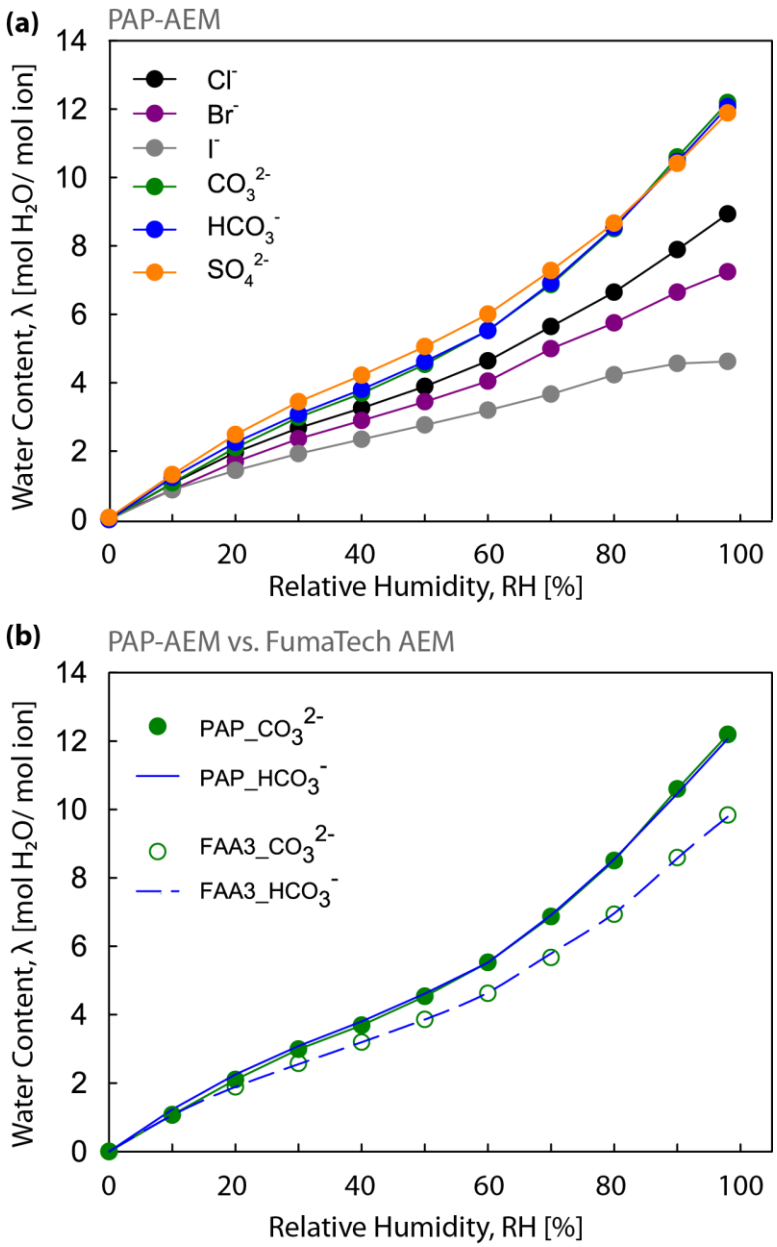

Figure 3 (a) Water content of PAP membranes at 25 °C based on the average of water content during sorption and desorption. (b) Water content comparison of PAP and FAA3 in carbonate and bicarbonate forms, where PAP obtains higher water content than FAA3.

Liquid and water vapor sorption are both relevant for AEMFCs as they often operate with humidified gases, which results in liquid water on the anodic side of the membrane, but water vapor on the cathodic side. To better understand AEMs' hydration behavior, their water uptakes in liquid water vs. saturated water vapor are compared in Figure 2. The water content (λ) of both

PAP and FAA3 membranes at 25 °C are higher in liquid water than at 100% RH, for all the anion forms investigated, a phenomenon frequently attributed to Schroeder's paradox. In addition, the difference in λ between liquid vs. vapor uptake (Δλ) exhibits dependence on the anion type (Figure 2b). Numerous studies reported that PFSA membranes show Schroeder's paradox; *i.e.*, membrane uptake in the liquid is higher than in saturated water vapor.[55-57] However, this effect was found to be absent in other membrane systems, such as disordered, sulfonated polystyrene-block-polyethylene copolymers.[58] Given that AEMs and sPEEK in this study also possess disordered nano-morphology (based on SAXS), their uptake can be analyzed to examine Schroeder's paradox. As shown in Figure 2b, all hydrocarbon ionomers (AEMs and sPEEK), regardless of counter-ion form, exhibit Schroeder's paradox, similar to PFSA-based ionomer systems, which can be attributed to the different structure rearrangements for the interface of membranes when exposed to liquid and water-vapor.[57, 59] Compared to Nafion, AEMs were found to have higher resistance to the surface rearrangements, due to its less well-structured membrane interface.[59]

3.2.2 Sorption hysteresis and swelling

Sorption hysteresis, in which the amount of the polar sorbate in the polymer in equilibrium with the external vapor is higher in desorption than in sorption mode, was observed in many polymeric materials upon swelling.[60] As shown in Figure 4, sorption hysteresis is observed for both PAP and FAA3 in the entire RH range with a maximum around 70% RH, where the membranes begin to exhibit nonlinear upturn in their sorption isotherms (Figure 3a). As will be discussed later, conductivity starts to increase dramatically at 70% RH as well. This is likely to be related to this transition in the hydration regime, where the onset of nonlinearity is usually associated with the structural changes (such as in phase-separated ionomers) or with the nature of water (water molecules more bound to cation sites vs. more free). In this study, given the lack of a structure, it could be attributed to the change in the nature of water, which agrees with the observation of maximum hysteresis, since the fluctuations in absorption of the free water during sorption vs desorption is expected in the proximity of this transition (~70% RH).

In HCO_3^- and CO_3^{2-} forms, AEMs exhibit larger humidity-induced hysteresis (Δ_{WU} is equivalent to λ = 2 mol H_2O/ mol Ion), which correlates well with their higher water content (Figure 3a) and bound (non-freezable) water (Table 2). This is a critical finding given that these anions are extensively involved in electrochemical systems such as alkaline fuel cells and electrolyzers, as

well as CO_2 reduction systems. The water sorption hysteresis is associated with the stress relaxation of the cohesive force opposing swelling.[60-61] In desorption mode, the bound water molecules keep the polymer chains apart, and the contractive forces are not sufficient to force the water molecules from the swollen structure as the water vapor pressure decreases, resulting in higher water content compared to that in sorption mode. The large sorption hysteresis was also found in weak polyelectrolytes, and other amorphous materials (*e.g.*, protein powder),[62-64] in which case the sorption hysteresis was attributed to the polymer's resistance to plasticization by water (i.e., stiffer chains) due to its higher shear modulus and the larger stress relaxation time consequently hampers the response to RH changes.[65]

While water content (λ) is used to describe the local hydration of ionomer moieties, water volume fraction, ϕ_w, is a better representation of the network-level properties.[49] Therefore, using both λ and ϕ_w can provide information about the local (nanoscale) vs. network (mesoscale) properties. The plot of water volume fraction, ϕ_w, as a function of λ often reveal insights into membrane swelling phenomena.[66-67] As shown in Figure 5, ϕ_w increases with λ for all ionomers, although ϕ_w is higher for PAP than FAA3 for each ion at a given λ, signifying larger swelling at the network level. This result is consistent with the higher swelling ratio of PAP in liquid water, as shown in Figure 7, which could be attributed to reduced hydrophobic segments in its polymer chain.

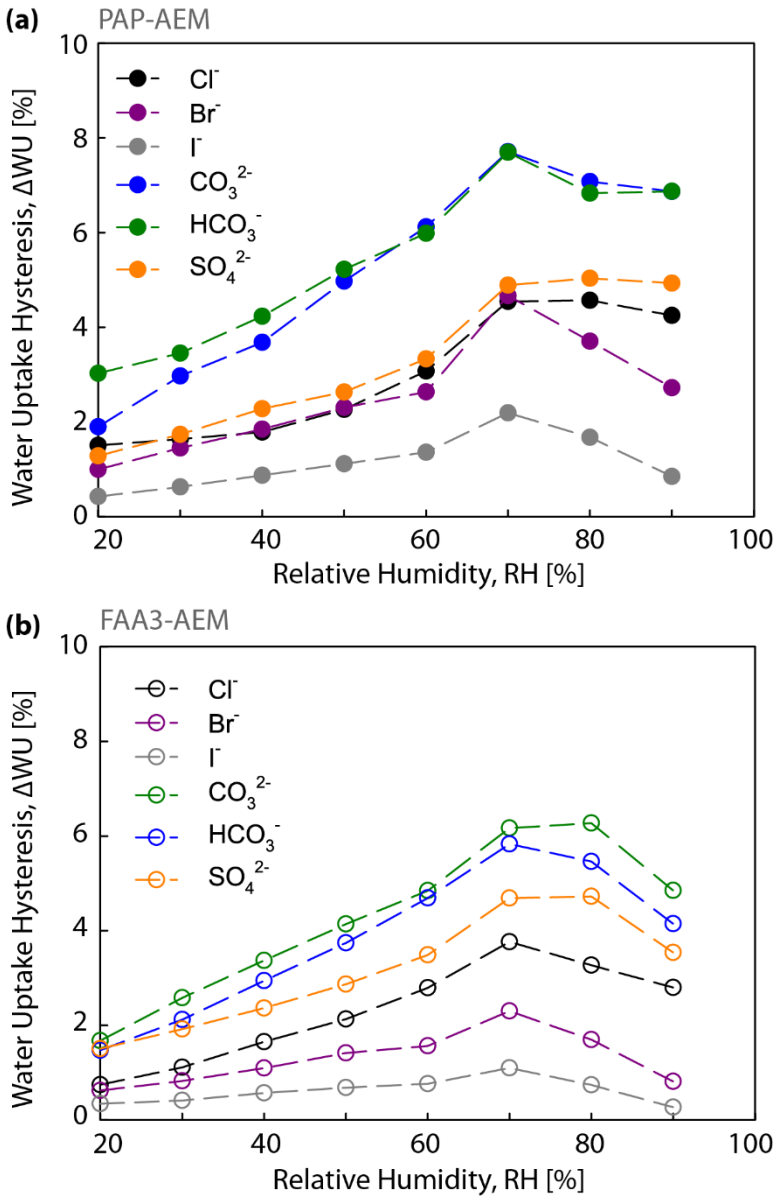

Figure 4 The hydration hysteresis (Δ_{WU}) shown in terms of the difference in percent weight change during desorption and sorption of (a) PAP and (b) FAA3 membrane in various counter-anions at 25°C.

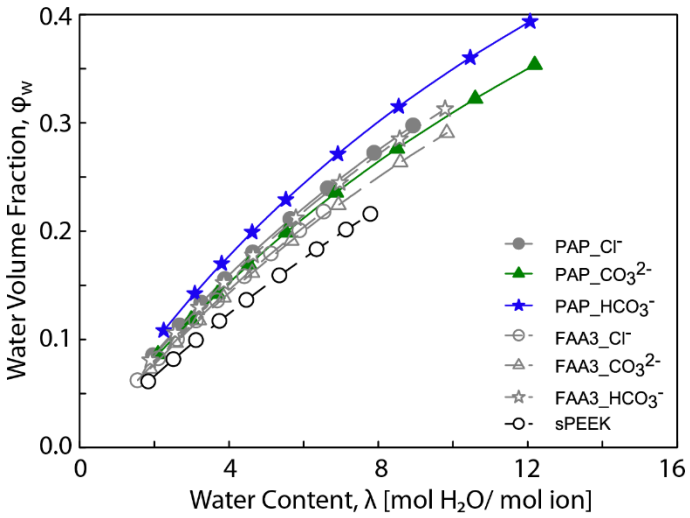

Figure 5 Relationship between water volume fraction and water content (λ) for the membranes determined from the measured gravimetric water uptake and density.

3.3 Anion conductivity

3.3.1 Ion conductivity in liquid water

The liquid-water conductivity of PAP and FAA3 in different anion forms are shown in Figure 6. Even though there was ~ 2 min air exposure and consequently carbonates formation[4] during the experiment, membranes in OH^- form (~7% OH^- converted to carbonates calculated according to ref.[68]) still exhibit the highest conductivity, which is expected given that OH^- anion has the highest mobility among the anions studied, due to its ability to exhibit structural diffusion (*e.g.*, ion hopping) (see Table 1). However, the difference in membrane conductivity between OH^- and other anions cannot be solely attributed to the ion mobility. For instance, in HCO_3^- form, the AEM conductivity decreases ten-fold compared to that in OH^- form, even though the mobility of the former is only five times higher at infinite dilution (Table 1). Kreuer et al. attributed this shift to the difference in the anions' enthalpies of dissolution due to anion binding to the cation in the polymer induced by ion size, resulting in a variation in the degree of ion dissociation.[4, 69] To examine this further, we plotted the anion conductivity as a function of anion radii in Figure 6c. It is shown that ion conductivity decreases with increasing radii of the anion of the same valence. Interestingly, anion valence also shows an impact on the ion conductivity. Conductivity normalized by conductivity with the infinite dilution of ions (κ/κ_o) is plotted in Figure 6b, where the I^- form shows the lowest value, as was the case with the conductivity (Figure 6a) which follows the same trend in Figure 6c.

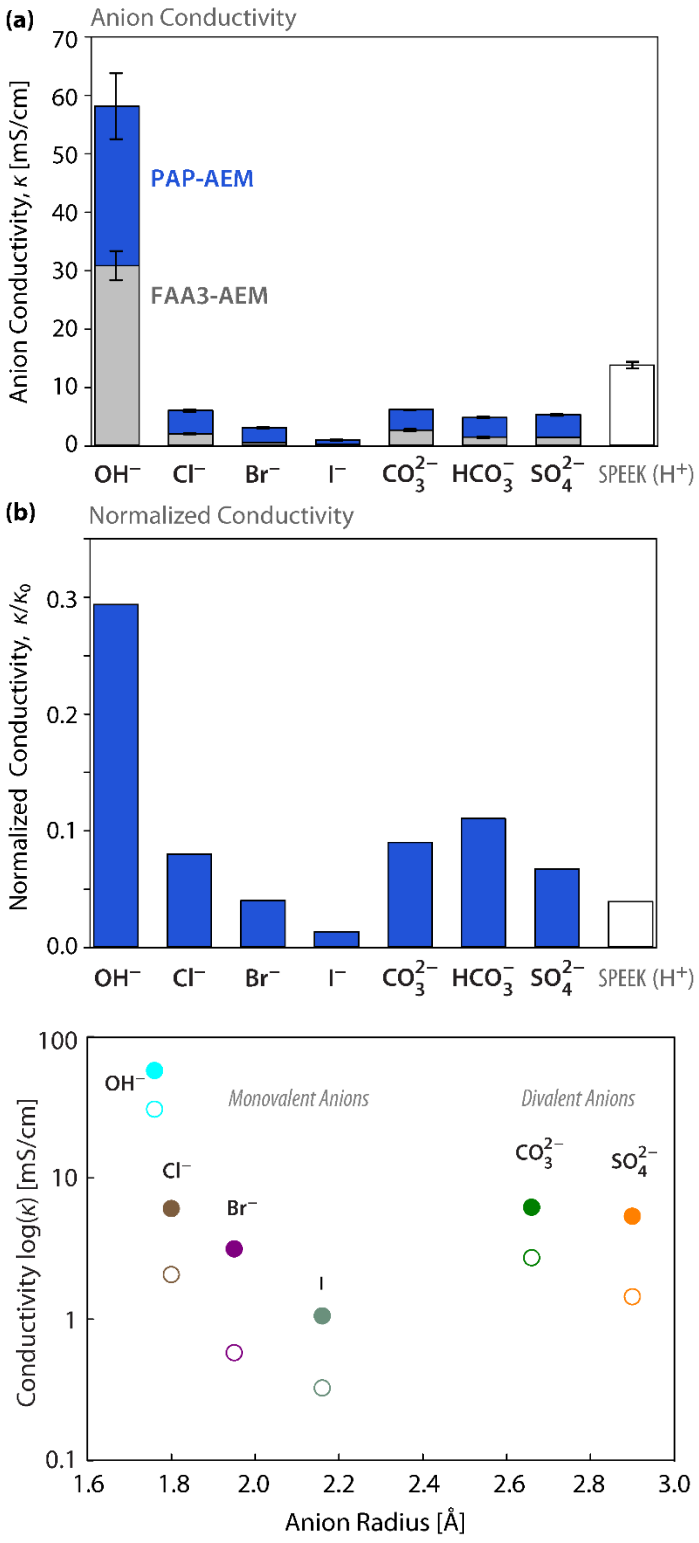

Figure 6 (a) Conductivity of PAP, FAA3, and sPEEK (H^+) membranes at 25 °C in liquid water; (b) the ratio of conductivity to the conductivity at infinite dilution of ions; (c) Conductivity plotted as a function of the anion size (radii values taken from ref.[70]). Solid symbols and open symbols correspond to PAP and FAA3, respectively.

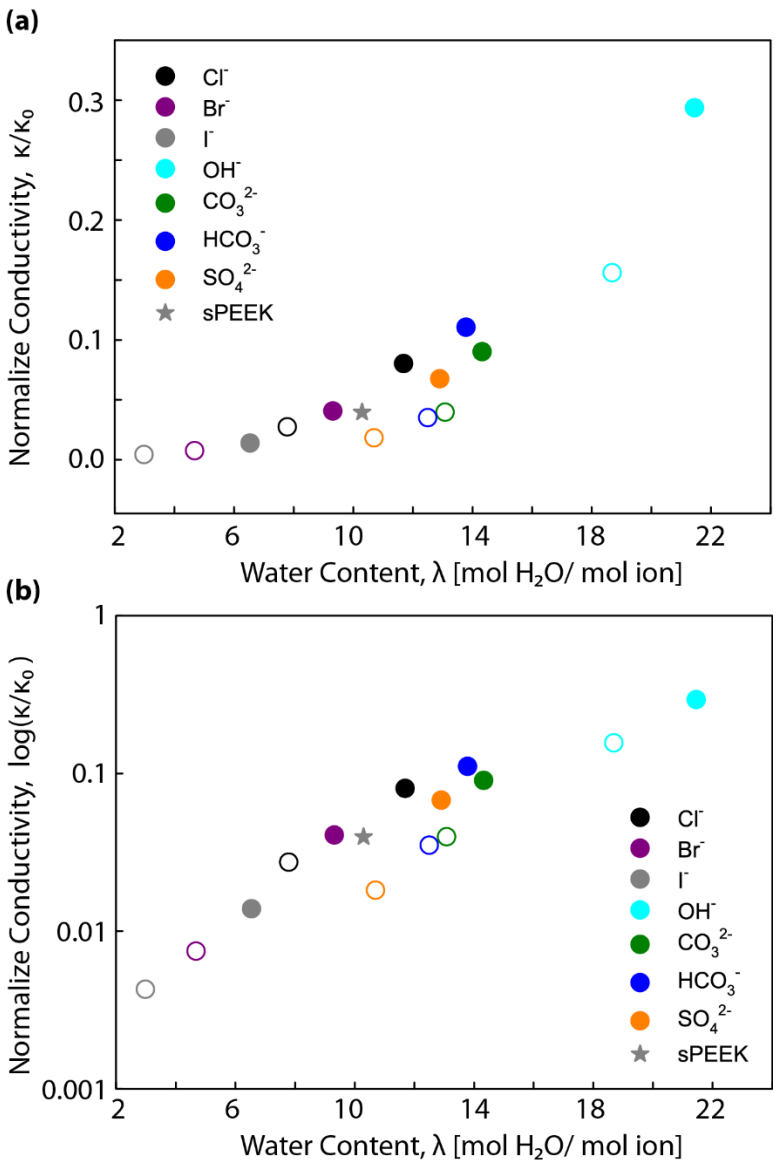

Figure 7 The ratio of conductivity to the conductivity at infinite dilution of ions (κ/κ_o) as a function of the water content of PAP (filled) and FAA3 (open) at 25 °C in liquid water, plotted in linear and log scale. Proton-form sPEEK data is included for comparison.

Compared to FAA3, PAP demonstrates much greater anion conductivity, towing to PAP-AEM's higher water content, λ, for each counter-anion (as shown in Figure 2). To examine the impact of hydration, effective conductivity, κ/κ_o, is plotted as a function of water content, as shown in (Figure 7). Overall, conductivity correlates fairly well with both water content and swelling ratio (Figure S3). Compared to sPEEK, two AEMs exhibit similar κ/κ_o values for a given water content, despite their higher IEC values. This could be attributed to these hydrocarbon polymers being in a

more amorphous mixed network morphology as evident from the lack of phase separation (shown in the SAXS data in Figure 1). The fact that κ/κ_o in liquid water shows a universal dependence on hydration, regardless of the ion form, in the absence of any discernible change in nano-morphology (Figure 1), illustrates that transport is hydration-controlled, in sharp contrast to phase-separated ionomers where ion transport is influenced by nanostructure-hydration interplay.[49] Our results are in line with recent simulation work,[71] where the transport properties of the AEM were found to be highly dependent on the hydration level but with much less sensitivity to polymer architecture.

3.3.2 Carbonate conductivity with humidity effect

AEM carbonation occurs in a CO_2-containing environment, which creates performance problems for AEMFC operation.[27] An AEM in OH^- form is chemically transformed through acid-base reactions, thereby creating bicarbonate (HCO_3^-) and carbonate (CO_3^{2-}) anions and consequently reducing membrane conductivity and overall AEMFC performance.[68, 72-73] Despite these limitations, the formation of carbonates can be useful for other electrochemical systems. Carbonates are weaker nucleophiles than hydroxide, meaning that membranes will be less prone to the chemical attacks in carbonate media than in hydroxide media.[74] This also indicates that systems with liquid feeds, like AEM-based electrolyzers, may last longer in the presence of some solubilized carbonate. Researchers have even proposed using carbonate purposefully for other applications, including electrochemical CO_2 separation.[75] It was shown by numerical simulations that carbonate form (CO_3^{2-}) is the dominate species inside the AEM during cell operation,[68, 76-78] therefore, we focused on CO_3^{2-} anion form and measured conductivity as a function of relative humidity. Due to the hysteresis observed in the AEM water sorption isotherms, anion conductivity is measured during humidification (sorption mode) and dehumidification (desorption mode) (Figure 8). Interestingly, conductivity is higher during dehumidification, which correlates with their higher water content under this mode (Figure 8b), which again signifies the importance of hydration to the conductivity of these AEMs. Moreover, Dekel and co-workers suggested that an AEM's chemical degradation could accelerate more at lower water content than at high water content, which enhances the shielding of the OH^- by the water molecules.[79-80] Therefore, our findings indicate measuring *ex-situ* AEM conductivity during dehydration mode from high RH could be a better diagnostic.

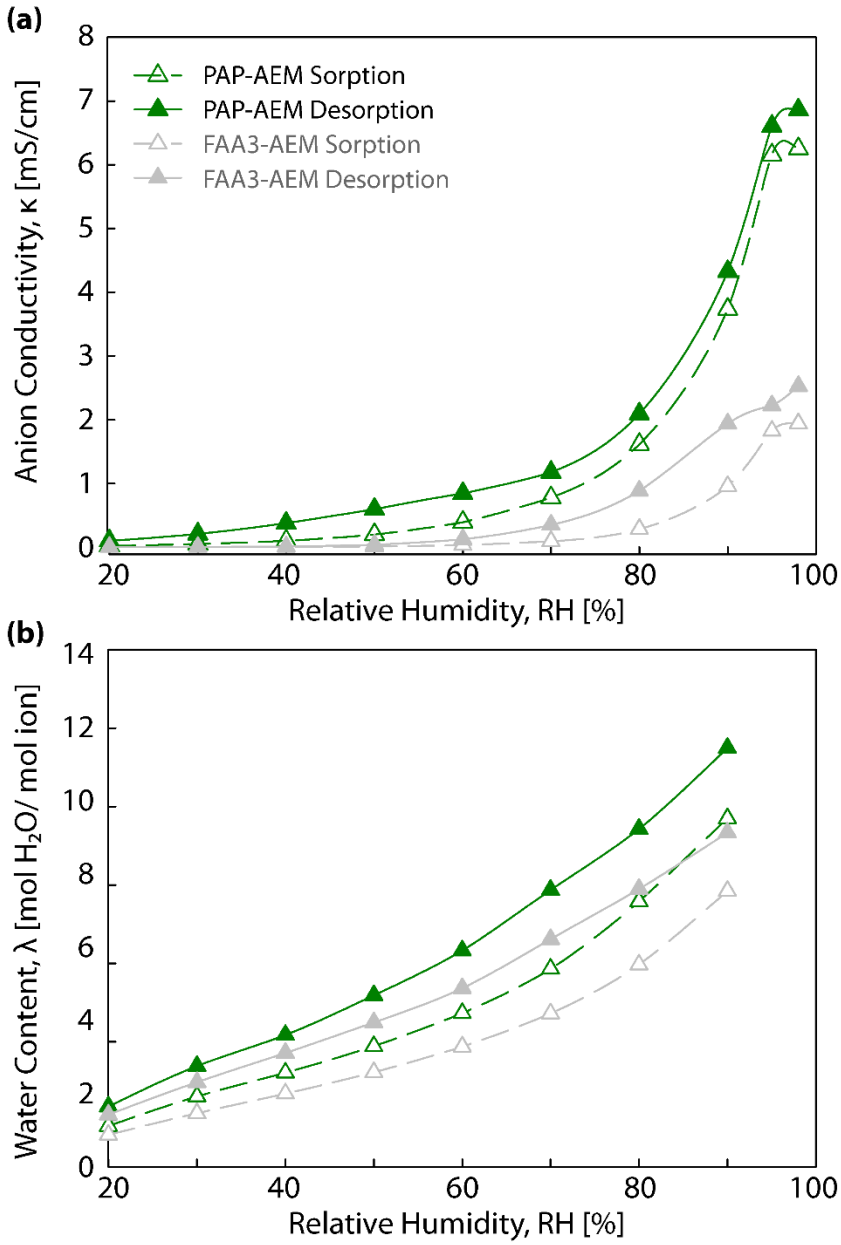

Figure 8 The impact of relative humidity on (a) conductivity and (b) water content of membranes in CO_3^{2-} form, during sorption and desorption at 30 °C.

Figure 9a compares the anion conductivity of membranes in HCO_3^-, CO_3^{2-} against Cl^- forms. PAP AEM exhibits lower conductivity in its carbonate forms than in Cl^- form for a given λ. Once λ exceeds 9, however, the trend reverses, and the AEMs in carbonate forms show higher conductivity, which highlights the importance of water content in ion conduction. A closer examination of data in Figure 9a reveals that the conductivity percolation threshold for AEMs shifts

to larger λ compared to that for Nafion (*i.e.*, λ = 2 mol H_2O/SO_3H), indicating that efficient anion dissociation in AEMs requires more water molecules. Also, compared to Nafion, the increase in conductivity of AEMs shows a weaker dependence on water content, *i.e.*, a smaller slope of κ vs. λ curve. Such a trend was shown to be related to the mesoscale effects and network connectivity in PFSAs.[66] Hence, in the absence of well-defined nanostructural transport pathways, these AEMs exhibit lower conductivity, which is controlled primarily by hydration. Interestingly, at intermediate hydration levels (λ > 6), the slope of κ vs. λ curves are similar for both Nafion and sPEEK, despite the lack of phase-separated morphology of the latter. Thus, while sPEEK and AEMs seemingly possess similar nano-morphology, the distinct change in their hydration-dependent conductivity underscores the difference in ion conduction mechanisms, namely, the protons vs. the anions. Underlying origins of this discrepancy can be explored by examining the factors controlling the conductivity.

In a polymer electrolyte membrane, ion transport is controlled by multiple factors, including ion concentration and mobility, tortuosity of transport pathways at the mesoscale, and electrostatic interactions and solvation energies at the nanoscale. Conductivity can be expressed in terms of concentration of mobile carriers ($[\phi^-]$)and effective ion mobility (μ_{X^-}) in the form of $\kappa = F \times [\phi^-] \times \mu_{X^-}$, where *F* denotes the Faraday constant. As shown in Figure 9b, despite having higher ion concentration than Nafion and sPEEK PEMs, PAP and FAA3 AEMs exhibit significantly lower ion mobility (Figure 10a inset) and therefore lower conductivity, which emphasizes the importance of mobility to the ion conduction. This finding holds with different counter-anions of AEMs, for instance, the CO_3^{2-} and HCO_3^- forms show similar conductivity, due to their similar ion mobility, despite the higher ion concentration of latter.

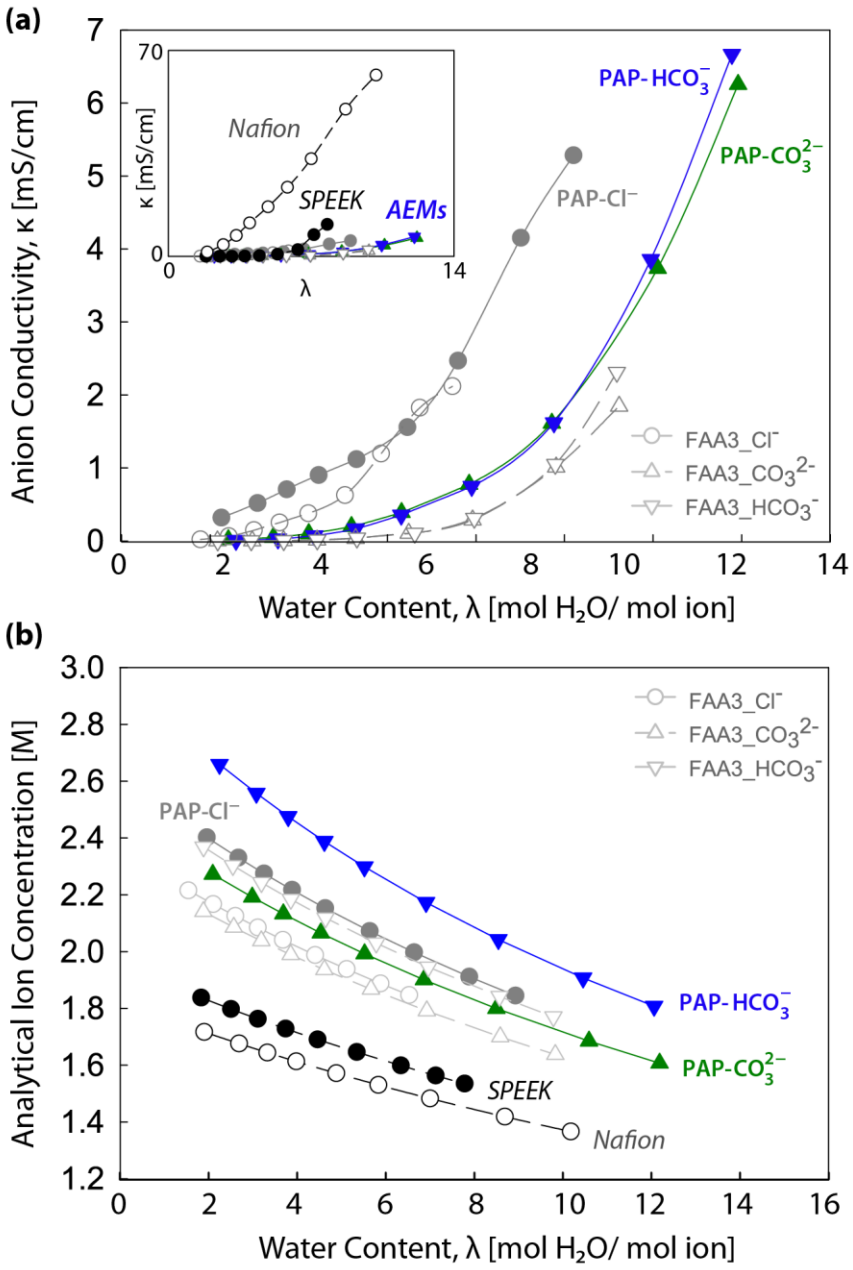

Figure 9 The impact of water content on (a) ion conductivity (b) analytical ion concentration of PAP and FAA3 at 30 °C. sPEEK and Nafion 211 are used for comparison. Legends are the same in a and b.

Figure 10b shows normalized ion mobility as a function of λ, compared to Nafion, AEMs and sPEEK exhibit lower normalized ion mobility for a given λ, which could be attributed, in part, to weakly-structured conductive pathways in AEMs as inferred from SAXS (Figure 1). Plotting data as a function of water volume fraction also shows similar trends (Figure S4). Interestingly,

the slope of normalized ion mobility vs. λ become similar for PEM and AEMs at higher hydration levels (Figure 10b), which indicate comparable network effects on ion diffusion once a hydrated network forms (at high λ). The fact that transport-hydration relationships vary from the nanoscale correlations (μ vs. λ) to mesoscale descriptions for normalized mobility (κ/κ$_o$ vs. λ or κ/κ$_o$ vs. ϕ_w, see Figure S4) highlights the role of nanostructure in ion conductivity, which is in line with previous efforts aiming to achieve well-connected ionic pathways.[11, 17-22, 81-83]

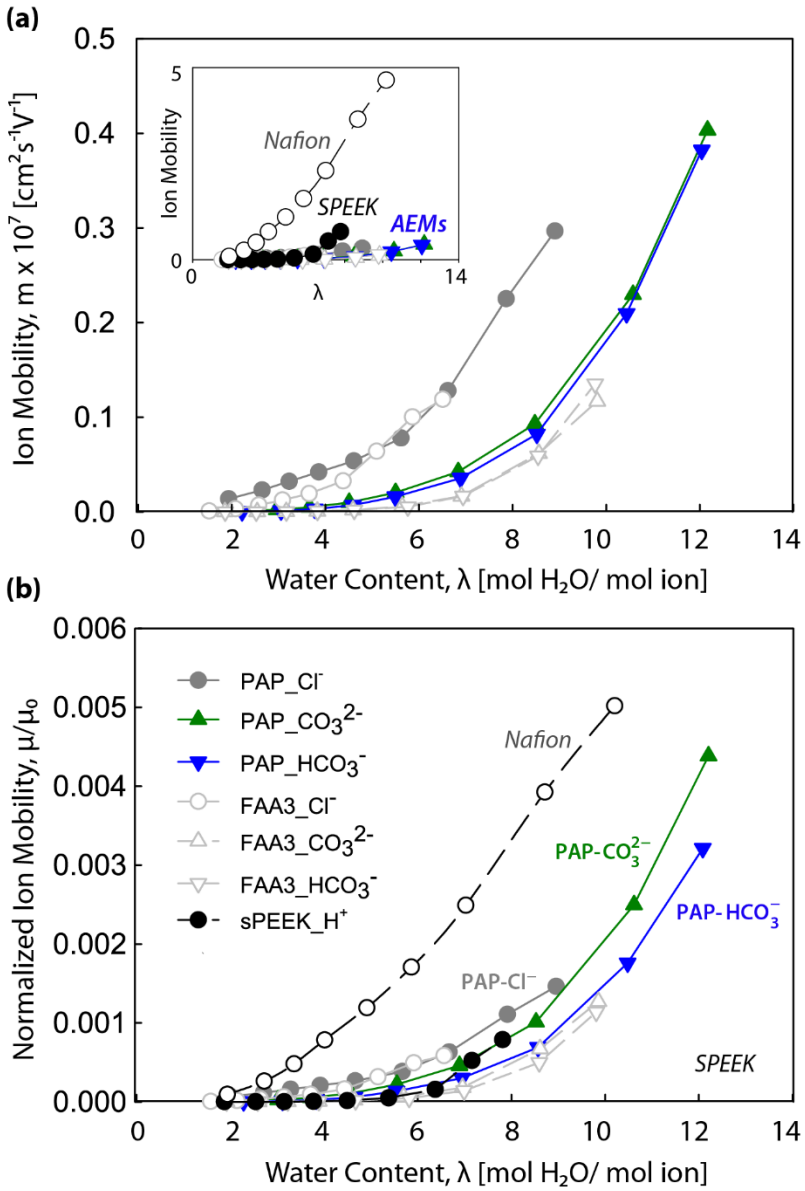

Figure 10 The impact of water content on (a) ion mobility (b) normalized ion mobility to mobility at infinite ion dilution (μ/μ$_o$) of PAP, FAA3 at 30 °C. sPEEK and Nafion 211 are used for comparison. Legends are the same in a and b.

3.3.3 Effect of temperature on conductivity

Despite improved cell performance at higher temperatures, most of the H_2-HEMFC tests are limited to low operating temperatures (mainly ≤ 60 °C) due to stability issues.[27] Therefore, it is practical to explore the effect of temperature on AEM conductivity at various RHs. In polymer electrolyte membranes, conductivity increases with temperature, due to increased ion-water mobility and segmental motions of the polymer chains.[49] However, as shown in Figure 11, AEM conductivity increases from 30 to 40 °C and levels off after 40 °C, and does not exhibit a typical Arrhenius relationship for most RH conditions, which agrees well with SAXS data showing a lack of temperature effect on membrane nano-morphology (Figure 1b). In contrast, RH (or hydration) has a strong effect on membrane conductivity. Comparison of the impact of humidity and temperature on anion conductivity reveals that hydration plays a more important role than the temperature in ion transport when the T > 40°C.

In the high RH regime (RH > 90%), the correlation of conductivity and temperature, however, exhibits Arrhenius-type behavior, which could be due to higher hydration. The activation energies (Ea) were obtained using ($\kappa = \mathrm{A}\, exp\left(-\frac{Ea}{RT}\right)$), where R is the gas constant (8.314 J/mol/K); A is a prefactor; and T is the temperature (K). At RH= 90%, Ea is calculated to be 15 kJ/mol, which is lower than literature values reported for poly(benzimidazolium) (PBI) based AEM.[84] The origins of such a discrepancy in Ea can be twofold: 1) differences in the chemical structure of polymers; 2) faster ion transport as a result of the short backbone allowing two QA groups from adjacent side chains to be in close proximity of each other, thereby making their first hydration shells overlap. [85-86]

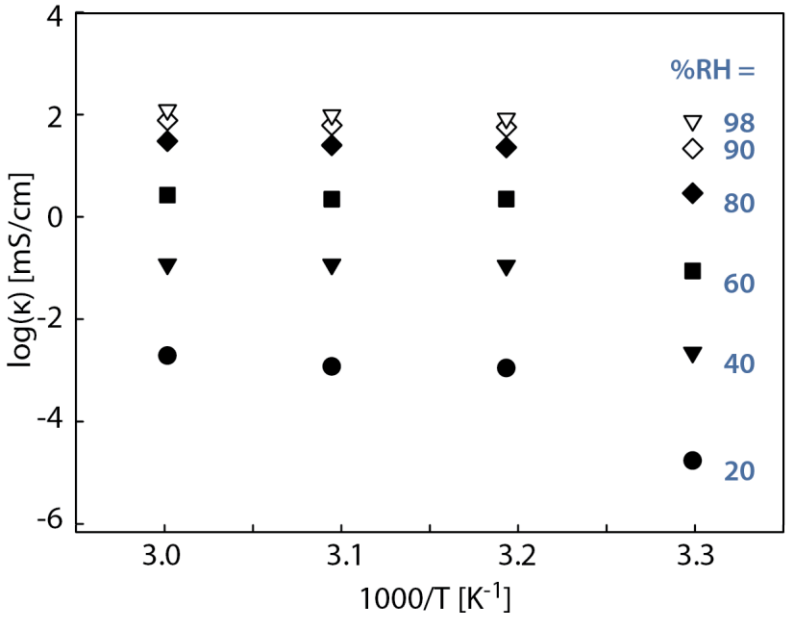

Figure 11 Conductivity of PAP-HCO_3^- as a function of temperature at various RH condition.

4. Conclusions

This study presents a systematic investigation of anion conductivity and water sorption of QA-based anion exchange membranes (AEMs) under liquid and water vapor conditions. We compared hydration and swelling behavior of poly(aryl-piperidinium)-based on terphenyl (PAP-TP-85) AEM against a commercial AEM (FAA3), as well as Nafion and sPEEK PEMs of varying degree of phase-separation to provide dual baselines. Small-angle X-ray scattering (SAXS) of the AEMs showed a very weak phase-separated nanostructure, regardless of their counter-anion form and hydration level. Also, the conductivity of these disordered AEMs and PEMs show a universal dependence on hydration level, indicating that transport is primarily hydration-controlled, in sharp contrast to strongly phase-separated ionomers (Nafion) where ion transport is influenced by nanostructure-hydration interplay.

The impact of counter-anion on water sorption and conductivity of these two AEMs is investigated to understand the transport in polymer electrolytes with disordered structure. Water content and ion conductivity of anions depends largely on the anion size, which could be associated with the dissolution enthalpy of counter-anions from the poly(cations) of the AEM. Comparing the water content in liquid vs. saturated vapor, both AEMs show an apparent difference, regardless of counter-anion form, is attributed to Schroeder's paradox observed in PEMs. AEMs in HCO_3^-

and CO_3^{2-} exhibit a larger humidity-induced hysteresis than do other anion form membranes. Anion transport measured at various hydration levels and temperatures show that water content plays a more significant role than the temperature in controlling the anion conductivity AEMs in water vapor. Despite their comparable disordered nano-morphology, PAP-AEM exhibits higher conductivity than FAA3, in all anion forms, due probably to its higher anion concentration. Within a disordered structure, AEM's conductivity is primarily governed by hydration, as opposed to phase-separated ion-exchange membranes wherein multi-scale morphology plays an additional role in altering hydration-transport interplay.

When comparing the two competing factors determining AEM conductivity, anion mobility plays a more significant role than anion concentration. When normalized ion mobility plotted against water content (λ), the initially lower slope of AEMs approaches that for PEMs with hydration, indicating comparable network effects on ion diffusion once a hydrated network forms. The fact that hydration-transport relationships vary largely from the nanoscale to mesoscale descriptions, highlights the role of nanostructure in ion conductivity. Collectively, this study demonstrates the importance of hydration level and ion mobility for anion transport in amorphous AEMs and provides further understanding into their structure-transport relationship, which shed light into the designing of AEMs with improved performance.

Acknowledgments

We thank Adam Z. Weber, Andrew Crothers, Michael Gerhardt, and Brian P. Setzler for their insightful reading of the manuscript and the helpful discussions. Funding for this work was provided by HyGEN Consortium through the Fuel Cell Technologies Office, Energy Efficiency and Renewable Energy Office, of the U.S. Department of Energy (DOE), under contract no. DE-AC02-05CH11231. We thank Chenhui Zhu and Eric Schaible for their assistance with facilitating the equipment at the Advanced Light Source (ALS) beamline 7.3.3, supported by the Office of Science, Office of Basic Energy Sciences, of the U.S. DOE (Contract No. DE-AC02-05CH11231).

References

1. Arges, C. G.; Zhang, L., Anion Exchange Membranes' Evolution toward High Hydroxide Ion Conductivity and Alkaline Resiliency. *ACS Applied Energy Materials* **2018,** *1* (7), 2991-3012.
2. Setzler, B. P.; Zhuang, Z.; Wittkopf, J. A.; Yan, Y., Activity targets for nanostructured platinum-group-metal-free catalysts in hydroxide exchange membrane fuel cells. *Nature Nanotechnology* **2016,** *11*, 1020.
3. He, Y.; Pan, J.; Wu, L.; Zhu, Y.; Ge, X.; Ran, J.; Yang, Z.; Xu, T., A Novel Methodology to Synthesize Highly Conductive Anion Exchange Membranes. *Scientific Reports* **2015,** *5*, 13417.
4. Marino, M. G.; Melchior, J. P.; Wohlfarth, A.; Kreuer, K. D., Hydroxide, halide and water transport in a model anion exchange membrane. *Journal of Membrane Science* **2014,** *464*, 61-71.
5. Li, N.; Leng, Y.; Hickner, M. A.; Wang, C.-Y., Highly Stable, Anion Conductive, Comb-Shaped Copolymers for Alkaline Fuel Cells. *Journal of the American Chemical Society* **2013,** *135* (27), 10124-10133.
6. Li, Y.; Xu, T.; Gong, M., Fundamental studies of a new series of anion exchange membranes: Membranes prepared from bromomethylated poly(2,6-dimethyl-1,4-phenylene oxide) (BPPO) and pyridine. *Journal of Membrane Science* **2006,** *279* (1), 200-208.
7. Wright, A. G.; Holdcroft, S., Hydroxide-Stable Ionenes. *ACS Macro Letters* **2014,** *3* (5), 444-447.
8. Varcoe, J. R.; Slade, R. C. T., An electron-beam-grafted ETFE alkaline anion-exchange membrane in metal-cation-free solid-state alkaline fuel cells. *Electrochemistry Communications* **2006,** *8* (5), 839-843.
9. Lee, W.-H.; Mohanty, A. D.; Bae, C., Fluorene-Based Hydroxide Ion Conducting Polymers for Chemically Stable Anion Exchange Membrane Fuel Cells. *ACS Macro Letters* **2015,** *4* (4), 453-457.
10. Dang, H. S.; Weiber, E. A.; Jannasch, P., Poly(phenylene oxide) functionalized with quaternary ammonium groups via flexible alkyl spacers for high-performance anion exchange membranes. *Journal of Materials Chemistry A* **2015,** *3* (10), 5280-5284.
11. Akiyama, R.; Yokota, N.; Otsuji, K.; Miyatake, K., Structurally Well-Defined Anion Conductive Aromatic Copolymers: Effect of the Side-Chain Length. *Macromolecules* **2018,** *51* (9), 3394-3404.
12. Kim, Y.; Moh, L. C. H.; Swager, T. M., Anion Exchange Membranes: Enhancement by Addition of Unfunctionalized Triptycene Poly(Ether Sulfone)s. *ACS Applied Materials & Interfaces* **2017,** *9* (49), 42409-42414.
13. Pan, J.; Li, Y.; Han, J.; Li, G.; Tan, L.; Chen, C.; Lu, J.; Zhuang, L., A strategy for disentangling the conductivity-stability dilemma in alkaline polymer electrolytes. *Energy and Environmental Science* **2013,** *6* (10), 2912-2915.
14. Wang, J.; Zhao, Y.; Setzler, B. P.; Rojas-Carbonell, S.; Ben Yehuda, C.; Amel, A.; Page, M.; Wang, L.; Hu, K.; Shi, L.; Gottesfeld, S.; Xu, B.; Yan, Y., Poly(aryl piperidinium) membranes and ionomers for hydroxide exchange membrane fuel cells. *Nature Energy* **2019**.
15. Fan, J.; Wright, A. G.; Britton, B.; Weissbach, T.; Skalski, T. J. G.; Ward, J.; Peckham, T. J.; Holdcroft, S., Cationic Polyelectrolytes, Stable in 10 M KOHaq at 100 °C. *ACS Macro Letters* **2017,** *6* (10), 1089-1093.
16. Hickner, M. A., Strategies for Developing New Anion Exchange Membranes and Electrode Ionomers. *The Electrochemical Society Interface* **2017,** *26* (1), 69-73.
17. Pan, J.; Chen, C.; Li, Y.; Wang, L.; Tan, L.; Li, G.; Tang, X.; Xiao, L.; Lu, J.; Zhuang, L., Constructing ionic highway in alkaline polymer electrolytes. *Energy & Environmental Science* **2014,** *7* (1), 354-360.
18. Ran, J.; Wu, L.; Wei, B.; Chen, Y.; Xu, T., Simultaneous Enhancements of Conductivity and Stability for Anion Exchange Membranes (AEMs) through Precise Structure Design. *Scientific Reports* **2014,** *4*, 6486.

19. Weiber, E. A.; Jannasch, P., Ion Distribution in Quaternary-Ammonium-Functionalized Aromatic Polymers: Effects on the Ionic Clustering and Conductivity of Anion-Exchange Membranes. *ChemSusChem* **2014,** *7* (9), 2621-2630.
20. Weiber, E. A.; Meis, D.; Jannasch, P., Anion conducting multiblock poly(arylene ether sulfone)s containing hydrophilic segments densely functionalized with quaternary ammonium groups. *Polymer Chemistry* **2015,** *6* (11), 1986-1996.
21. Li, N.; Wang, L.; Hickner, M., Cross-linked comb-shaped anion exchange membranes with high base stability. *Chemical Communications* **2014,** *50* (31), 4092-4095.
22. Si, J.; Lu, S.; Xu, X.; Peng, S.; Xiu, R.; Xiang, Y., A Gemini quaternary ammonium poly (ether ether ketone) anion-exchange membrane for alkaline fuel cell: Design, synthesis, and properties. *ChemSusChem* **2014,** *7* (12), 3389-3395.
23. Omasta, T. J.; Park, A. M.; LaManna, J. M.; Zhang, Y.; Peng, X.; Wang, L.; Jacobson, D. L.; Varcoe, J. R.; Hussey, D. S.; Pivovar, B. S.; Mustain, W. E., Beyond catalysis and membranes: visualizing and solving the challenge of electrode water accumulation and flooding in AEMFCs. *Energy & Environmental Science* **2018,** *11* (3), 551-558.
24. Park, C. H.; Lee, S. Y.; Hwang, D. S.; Shin, D. W.; Cho, D. H.; Lee, K. H.; Kim, T.-W.; Kim, T.-W.; Lee, M.; Kim, D.-S.; Doherty, C. M.; Thornton, A. W.; Hill, A. J.; Guiver, M. D.; Lee, Y. M., Nanocrack-regulated self-humidifying membranes. *Nature* **2016,** *532*, 480.
25. Omasta, T. J.; Wang, L.; Peng, X.; Lewis, C. A.; Varcoe, J. R.; Mustain, W. E., Importance of balancing membrane and electrode water in anion exchange membrane fuel cells. *Journal of Power Sources* **2018,** *375*, 205-213.
26. Dekel, D. R.; Rasin, I. G.; Brandon, S., Predicting performance stability of anion exchange membrane fuel cells. *Journal of Power Sources* **2019,** *420*, 118-123.
27. Dekel, D. R., Review of cell performance in anion exchange membrane fuel cells. *Journal of Power Sources* **2018,** *375*, 158-169.
28. Cho, M. K.; Park, H.-Y.; Lee, H. J.; Kim, H.-J.; Lim, A.; Henkensmeier, D.; Yoo, S. J.; Kim, J. Y.; Lee, S. Y.; Park, H. S.; Jang, J. H., Alkaline anion exchange membrane water electrolysis: Effects of electrolyte feed method and electrode binder content. *Journal of Power Sources* **2018,** *382*, 22-29.
29. Schwenzer, B.; Zhang, J.; Kim, S.; Li, L.; Liu, J.; Yang, Z., Membrane Development for Vanadium Redox Flow Batteries. *ChemSusChem* **2011,** *4* (10), 1388-1406.
30. Kutz, R. B.; Chen, Q.; Yang, H.; Sajjad, S. D.; Liu, Z.; Masel, I. R., Sustainion Imidazolium-Functionalized Polymers for Carbon Dioxide Electrolysis. *Energy Technology* **2017,** *5* (6), 929-936.
31. Bruce, P. G.; Freunberger, S. A.; Hardwick, L. J.; Tarascon, J.-M., Li–O2 and Li–S batteries with high energy storage. *Nature Materials* **2011,** *11*, 19.
32. Zheng, Y.; Ash, U.; Pandey, R. P.; Ozioko, A. G.; Ponce-González, J.; Handl, M.; Weissbach, T.; Varcoe, J. R.; Holdcroft, S.; Liberatore, M. W.; Hiesgen, R.; Dekel, D. R., Water Uptake Study of Anion Exchange Membranes. *Macromolecules* **2018**.
33. Luo, X.; Wright, A.; Weissbach, T.; Holdcroft, S., Water permeation through anion exchange membranes. *Journal of Power Sources* **2018,** *375* (Supplement C), 442-451.
34. Li, Y. S.; Zhao, T. S.; Yang, W. W., Measurements of water uptake and transport properties in anion-exchange membranes. *International Journal of Hydrogen Energy* **2010,** *35* (11), 5656-5665.
35. Peng, J.; Roy, A. L.; Greenbaum, S. G.; Zawodzinski, T. A., Effect of CO2 absorption on ion and water mobility in an anion exchange membrane. *Journal of Power Sources* **2018,** *380*, 64-75.
36. Yoshimura, K.; Zhao, Y.; Hasegawa, S.; Hiroki, A.; Kishiyama, Y.; Shishitani, H.; Yamaguchi, S.; Tanaka, H.; Koizumi, S.; Appavou, M.-S.; Radulescu, A.; Richter, D.; Maekawa, Y., Imidazolium-based anion exchange membranes for alkaline anion fuel cells: (2) elucidation of the ionic structure and its impact on conducting properties. *Soft Matter* **2017,** *13* (45), 8463-8473.

37. Schibli, E. M.; Wright, A. G.; Holdcroft, S.; Frisken, B. J., Morphology of Anion-Conducting Ionenes Investigated by X-ray Scattering and Simulation. *The Journal of Physical Chemistry B* **2018,** *122* (5), 1730-1737.
38. Zhao, Y.; Yoshimura, K.; Yu, H.-C.; Maekawa, Y.; Hiroki, A.; Kishiyama, Y.; Shishitani, H.; Yamaguchi, S.; Tanaka, H.; Koizumi, S.; Appavou, M.-S.; Houston, J.; Radulescu, A.; Richter, D., Small angle neutron scattering study on the morphology of imidazolium-based grafted anion-conducting fuel cell membranes. *Physica B: Condensed Matter* **2018**.
39. Kreuer, K.-D., Ion Conducting Membranes for Fuel Cells and other Electrochemical Devices. *Chemistry of Materials* **2014,** *26* (1), 361-380.
40. Guo, D.; Lin, C. X.; Hu, E. N.; Shi, L.; Soyekwo, F.; Zhang, Q. G.; Zhu, A. M.; Liu, Q. L., Clustered multi-imidazolium side chains functionalized alkaline anion exchange membranes for fuel cells. *Journal of Membrane Science* **2017,** *541*, 214-223.
41. He, Y.; Si, J.; Wu, L.; Chen, S.; Zhu, Y.; Pan, J.; Ge, X.; Yang, Z.; Xu, T., Dual-cation comb-shaped anion exchange membranes: Structure, morphology and properties. *Journal of Membrane Science* **2016,** *515*, 189-195.
42. Shi, S.; Weber, A. Z.; Kusoglu, A., STRUCTURE-TRANSPORT RELATIONSHIP OF PERFLUOROSULFONIC-ACID MEMBRANES IN DIFFERENT CATIONIC FORMS. *Electrochimica Acta* **2016,** *220*, 517-528.
43. Zhu, Z.; Luo, X.; Paddison, S. J., DPD simulations of anion exchange membranes functionalized with various cationic groups and associated anions. *Solid State Ionics* **2019,** *340*, 115011.
44. Luo, X.; Ghassemzadeh, L.; Holdcroft, S., Effect of free radical-induced degradation on water permeation through PFSA ionomer membranes. *International Journal of Hydrogen Energy* **2015,** *40* (46), 16714-16723.
45. Shi, S.; Weber, A. Z.; Kusoglu, A., Structure/property relationship of Nafion XL composite membranes. *Journal of Membrane Science* **2016,** *516*, 123-134.
46. Hatakeyama, T.; Nakamura, K.; Hatakeyama, H., Determination of bound water content in polymers by DTA, DSC and TG. *Thermochimica Acta* **1988,** *123*, 153-161.
47. Siu, A.; Schmeisser, J.; Holdcroft, S., Effect of Water on the Low Temperature Conductivity of Polymer Electrolytes. *The Journal of Physical Chemistry B* **2006,** *110* (12), 6072-6080.
48. Wang, W. Y.; Li, A. M.; Zhang, X. M., DSC and SEM Analysis on Bound Water Characteristics in Sewage Sludge. *Advanced Materials Research* **2012,** *347-353*, 2085-2089.
49. Kusoglu, A.; Weber, A. Z., New Insights into Perfluorinated Sulfonic-Acid Ionomers. *Chemical Reviews* **2017,** *117* (3), 987-1104.
50. Mandal, M.; Huang, G.; Kohl, P. A., Highly Conductive Anion-Exchange Membranes Based on Cross-Linked Poly(norbornene): Vinyl Addition Polymerization. *ACS Applied Energy Materials* **2019,** *2* (4), 2447-2457.
51. Haynes, W. M., *CRC handbook of Chemistry and Physics*. 93 rd ed.; 2012.
52. Detallante, V.; Langevin, D.; Chappey, C.; Métayer, M.; Mercier, R.; Pinéri, M., Water vapor sorption in naphthalenic sulfonated polyimide membranes. *Journal of Membrane Science* **2001,** *190* (2), 227-241.
53. Legras, M.; Hirata, Y.; Nguyen, Q. T.; Langevin, D.; Métayer, M., Sorption and diffusion behaviors of water in Nation 117 membranes with different counter ions. *Desalination* **2002,** *147* (1), 351-357.
54. Yadav, S.; Chandra, A., Structural and Dynamical Nature of Hydration Shells of the Carbonate Ion in Water: An Ab Initio Molecular Dynamics Study. *The Journal of Physical Chemistry B* **2018,** *122* (4), 1495-1504.
55. Weber, A. Z.; Newman, J., Transport in Polymer-Electrolyte Membranes: I. Physical Model. *J Electrochem Soc* **2003,** *150* (7), A1008-A1015.

56. Bass, M.; Freger, V., An experimental study of Schroeder's paradox in Nafion and Dowex polymer electrolytes. *Desalination* **2006,** *199* (1–3), 277-279.
57. Freger, V., Hydration of Ionomers and Schroeder's Paradox in Nafion. *The Journal of Physical Chemistry B* **2009,** *113* (1), 24-36.
58. Beers, K. M.; Yakovlev, S.; Jackson, A.; Wang, X.; Hexemer, A.; Downing, K. H.; Balsara, N. P., Absence of Schroeder's Paradox in a Nanostructured Block Copolymer Electrolyte Membrane. *The Journal of Physical Chemistry B* **2014,** *118* (24), 6785-6791.
59. Luo, X.; Wright, A.; Weissbach, T.; Holdcroft, S., Water permeation through anion exchange membranes. *Journal of Power Sources* **2018,** *375*, 442-451.
60. Watt, I. C., Adsorption-Desorption Hysteresis in Polymers. *Journal of Macromolecular Science: Part A - Chemistry* **1980,** *14* (2), 245-255.
61. Jeromenok, J.; Weber, J., Restricted Access: On the Nature of Adsorption/Desorption Hysteresis in Amorphous, Microporous Polymeric Materials. *Langmuir : the ACS journal of surfaces and colloids* **2013,** *29* (42), 12982-12989.
62. Palmer, J. C.; Debenedetti, P. G., Computer Simulation of Water Sorption on Flexible Protein Crystals. *The Journal of Physical Chemistry Letters* **2012,** *3* (18), 2713-2718.
63. Kim, S. B.; Singh, R. S.; Paul, P. K. C.; Debenedetti, P. G., Effects of disulfide bridges and backbone connectivity on water sorption by protein matrices. *Scientific Reports* **2017,** *7* (1), 7957.
64. Bryan, W. P., Thermodynamic models for water–protein sorption hysteresis. *Biopolymers* **1987,** *26* (10), 1705-1716.
65. Lee, S.-W.; Lee, D., Integrated Study of Water Sorption/Desorption Behavior of Weak Polyelectrolyte Layer-by-Layer Films. *Macromolecules* **2013,** *46* (7), 2793-2799.
66. Luo, X.; Holdcroft, S.; Mani, A.; Zhang, Y.; Shi, Z., Water, proton, and oxygen transport in high IEC, short side chain PFSA ionomer membranes: consequences of a frustrated network. *Physical Chemistry Chemical Physics* **2011,** *13* (40), 18055-18062.
67. Peckham, T. J.; Schmeisser, J.; Holdcroft, S., Relationships of Acid and Water Content to Proton Transport in Statistically Sulfonated Proton Exchange Membranes: Variation of Water Content Via Control of Relative Humidity. *The Journal of Physical Chemistry B* **2008,** *112* (10), 2848-2858.
68. Ziv, N.; Mustain, W. E.; Dekel, D. R., The Effect of Ambient Carbon Dioxide on Anion-Exchange Membrane Fuel Cells. *ChemSusChem* **2018,** *11* (7), 1136-1150.
69. Pearson, R. G., Hard and Soft Acids and Bases. *Journal of the American Chemical Society* **1963,** *85* (22), 3533-3539.
70. Nightingale, E. R., Phenomenological Theory of Ion Solvation. Effective Radii of Hydrated Ions. *The Journal of Physical Chemistry* **1959,** *63* (9), 1381-1387.
71. Lu, J.; Barnett, A.; Molinero, V., Effect of Polymer Architecture on the Nanophase Segregation, Ionic Conductivity, and Electro-Osmotic Drag of Anion Exchange Membranes. *The Journal of Physical Chemistry C* **2019,** *123* (14), 8717-8726.
72. Gerhardt, M. R.; Pant, L. M.; Weber, A. Z., Along-the-Channel Impacts of Water Management and Carbon-Dioxide Contamination in Hydroxide-Exchange-Membrane Fuel Cells: A Modeling Study. *Journal of The Electrochemical Society* **2019,** *166* (7), F3180-F3192.
73. Zheng, Y.; Omasta, T. J.; Peng, X.; Wang, L.; Varcoe, J. R.; Pivovar, B. S.; Mustain, W. E., Quantifying and elucidating the effect of CO2 on the thermodynamics, kinetics and charge transport of AEMFCs. *Energy & Environmental Science* **2019**.
74. Vega, J. A.; Chartier, C.; Mustain, W. E., Effect of hydroxide and carbonate alkaline media on anion exchange membranes. *Journal of Power Sources* **2010,** *195* (21), 7176-7180.
75. Omasta, T. J.; Mustain, W. E., Water and Ion Transport in Anion Exchange Membrane Fuel Cells. In *Anion Exchange Membrane Fuel Cells: Principles, Materials and Systems*, An, L.; Zhao, T. S., Eds. Springer International Publishing: Cham, 2018; pp 1-31.

76. Krewer, U.; Weinzierl, C.; Ziv, N.; Dekel, D. R., Impact of carbonation processes in anion exchange membrane fuel cells. *Electrochimica Acta* **2018,** *263*, 433-446.
77. Divekar, A. G.; Pivovar, B. S.; Herring, A. M., Kinetic Equilibrium Study of CO2 Poisoning Observed in Anion Exchange Membranes When Exposed to Ambient Air and Varying Levels of CO2 ppm. *ECS Transactions* **2018,** *86* (13), 643-648.
78. Weng, L.-C.; Bell, A. T.; Weber, A. Z., Towards membrane-electrode assembly systems for CO2 reduction: a modeling study. *Energy & Environmental Science* **2019,** *12* (6), 1950-1968.
79. Diesendruck, C. E.; Dekel, D. R., Water – A key parameter in the stability of anion exchange membrane fuel cells. *Current Opinion in Electrochemistry* **2018,** *9*, 173-178.
80. Dekel, D. R.; Amar, M.; Willdorf, S.; Kosa, M.; Dhara, S.; Diesendruck, C. E., Effect of Water on the Stability of Quaternary Ammonium Groups for Anion Exchange Membrane Fuel Cell Applications. *Chemistry of Materials* **2017,** *29* (10), 4425-4431.
81. Li, N.; Leng, Y.; Hickner, M. A.; Wang, C. Y., Highly stable, anion conductive, comb-shaped copolymers for alkaline fuel cells. *Journal of the American Chemical Society* **2013,** *135* (27), 10124-10133.
82. Sun, H.; Zhang, G.; Liu, Z.; Zhang, N.; Zhang, L.; Ma, W.; Zhao, C.; Qi, D.; Li, G.; Na, H., Self-crosslinked alkaline electrolyte membranes based on quaternary ammonium poly (ether sulfone) for high-performance alkaline fuel cells. *International Journal of Hydrogen Energy* **2012,** *37* (12), 9873-9881.
83. Rao, A. H. N.; Nam, S.; Kim, T. H., Comb-shaped alkyl imidazolium-functionalized poly(arylene ether sulfone)s as high performance anion-exchange membranes. *Journal of Materials Chemistry A* **2015,** *3* (16), 8571-8580.
84. Wright, A. G.; Fan, J.; Britton, B.; Weissbach, T.; Lee, H.-F.; Kitching, E. A.; Peckham, T. J.; Holdcroft, S., Hexamethyl-p-terphenyl poly(benzimidazolium): a universal hydroxide-conducting polymer for energy conversion devices. *Energy & Environmental Science* **2016,** *9* (6), 2130-2142.
85. Pandey, T. P.; Sarode, H. N.; Yang, Y.; Yang, Y.; Vezzù, K.; Noto, V. D.; Seifert, S.; Knauss, D. M.; Liberatore, M. W.; Herring, A. M., A Highly Hydroxide Conductive, Chemically Stable Anion Exchange Membrane, Poly(2,6 dimethyl 1,4 phenylene oxide)-b-Poly(vinyl benzyl trimethyl ammonium), for Electrochemical Applications. *J Electrochem Soc* **2016,** *163* (7), H513-H520.
86. Chen, C.; Tse, Y.-L. S.; Lindberg, G. E.; Knight, C.; Voth, G. A., Hydroxide Solvation and Transport in Anion Exchange Membranes. *Journal of the American Chemical Society* **2016,** *138* (3), 991-1000.

Appendix A

Additional data supporting the findings and discussions in the manuscript are presented, including the SAXS spectra of dry and wet PAP and FAA3 AEMs in different anions forms (Figure S1), water sorption data of FAA3 shown for various anions forms and compared to proton-form Nafion membranes (Figure S2), conductivity of the AEMs studied in this work plotted as a function of swelling (Figure S3), and the normalized ion mobility of PAP and FAA3 as a function of water volume fraction (Figure S4).

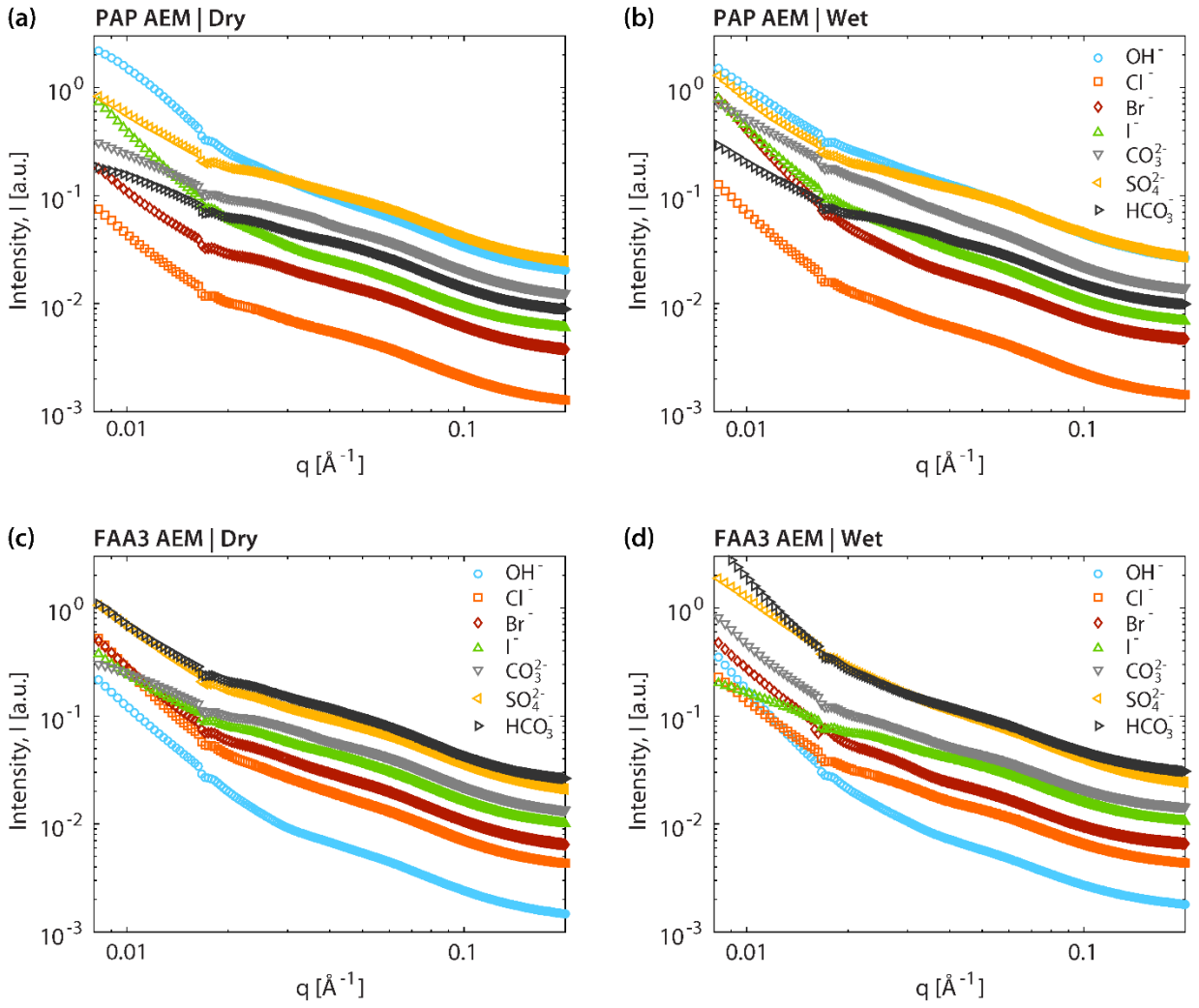

Figure S1 Small-angle X-ray scattering data for PAP (a ,b) and FAA3 (c, d) in various counter-anion forms under dry (a,c) and wet (b,d) conditions. FumaTech FAA3 membrane exhibits a broad SAXS peak around q = 0.5 - 0.6 Å^{-1} in both dry and wet state, indicating lack of an apparent nano-structural change with hydration. Moreover, the FAA3 shows similar SAXS features in all anions forms, with the exception of Br^- and I^-, for which another smaller broad peak emerges in water at q = 0.25 Å^{-1}.

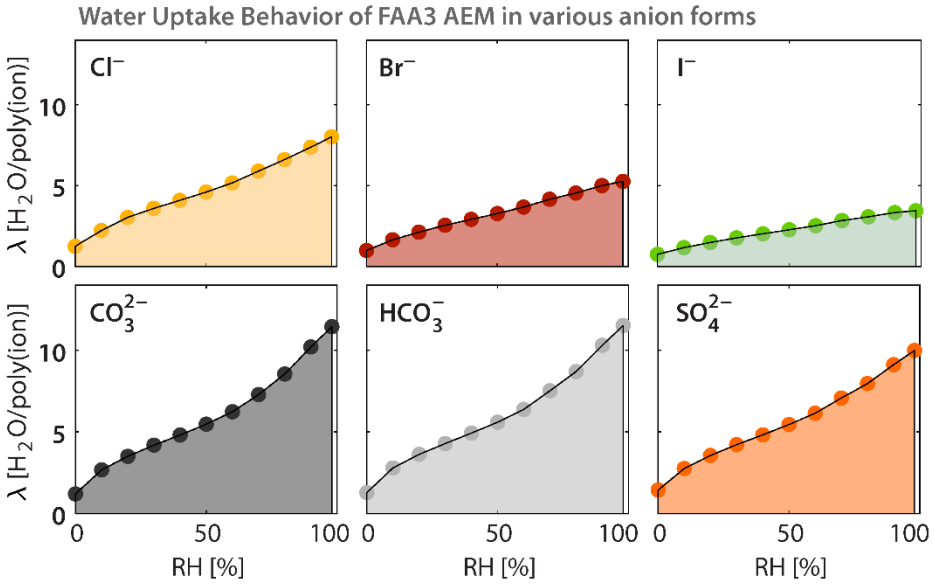

Figure S2 Water content as a function of relative humidity at 25 °C for FAA3 membranes.

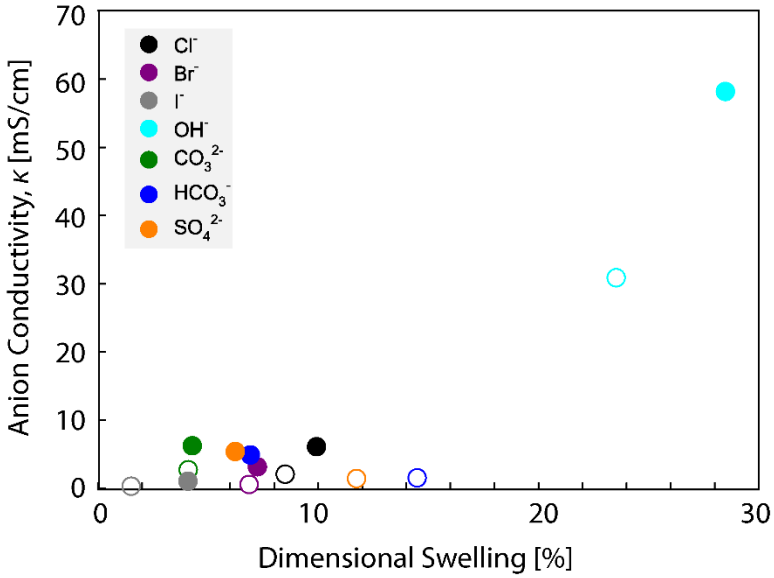

Figure S3 Conductivity as a function of swelling ratio of PAP (filled) and FAA3 (open) at 25 °C in liquid water.

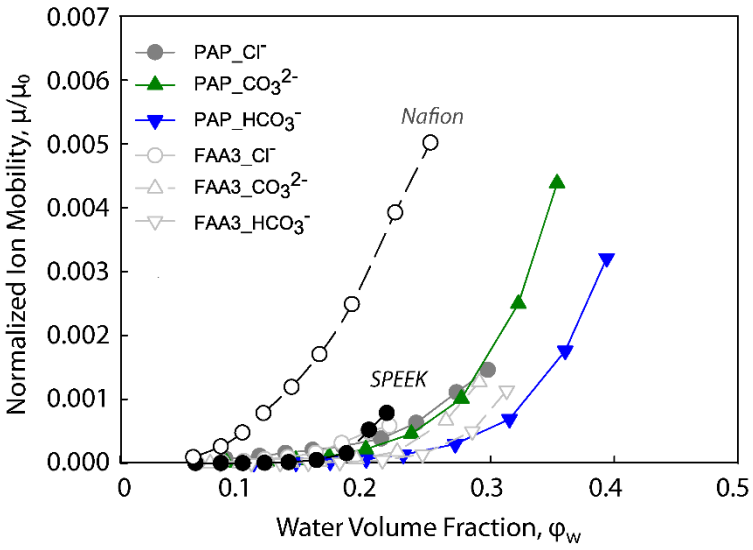

Figure S4 The impact of water volume fraction on normalized ion mobility to mobility at infinite ion dilution (μ/μ_o) of PAP and FAA3 at 30 °C. sPEEK and Nafion 211 are used for comparison.

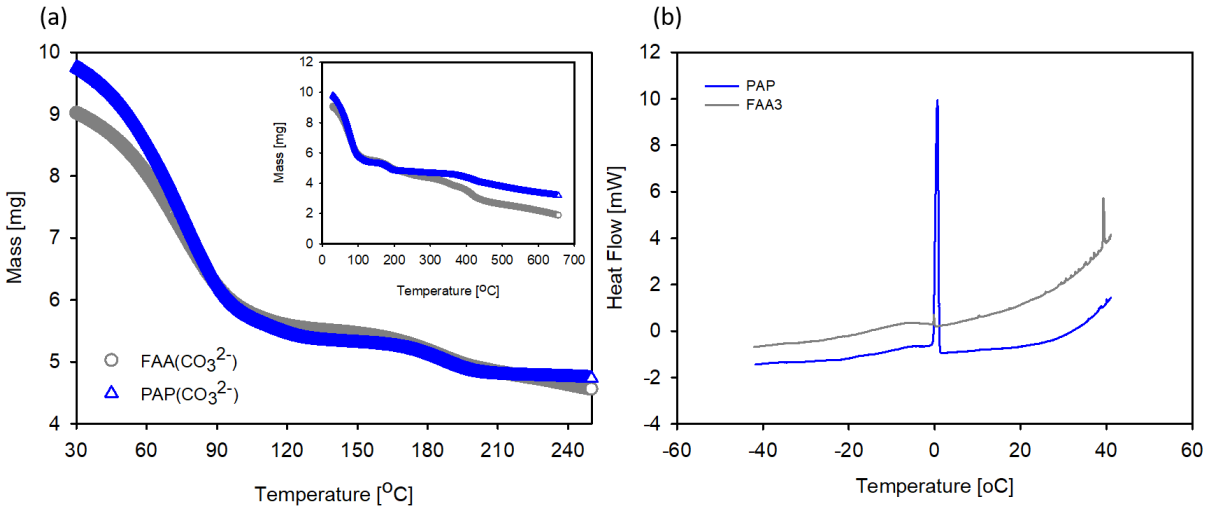

Figure S5 (a) TGA graphs and (b) DSC for hydrated PAP and FAA3 in carbonate ion form.